



Consumption and displacement speeds of stretched premixed flames – Theory and simulations



George K. Giannakopoulos^{a,*}, Christos E. Frouzakis^a, Shikhar Mohan^b, Ananias G. Tomboulides^c, Moshe Matalon^b

^a Aerothermochemistry and Combustion Systems Laboratory, ETH Zurich, Switzerland

^b Department of Mechanical Science and Engineering, University of Illinois, Urbana-Champaign, USA

^c Department of Mechanical Engineering, Aristotle University of Thessaloniki, Greece

ARTICLE INFO

Article history:

Received 11 November 2018

Revised 14 January 2019

Accepted 26 June 2019

Available online 11 July 2019

Keywords:

Flame displacement speed

Flame consumption speed

Global consumption rate

Spherical flame

Darrieus-Landau cusp flame

ABSTRACT

The flame displacement speed (FDS) and flame consumption speed (FCS) are commonly used in numerical studies to characterize flame dynamics. Although for a planar configuration they are both well defined and accurately represent the propagation speed of the flame into the combustible mixture, their definition in more general circumstances is ambiguous. The FDS and FCS are *local quantities*: the FDS is associated with the displacement of an arbitrarily selected iso-surface, and the FCS is an integrated quantity throughout a region that needs to be approximated, in a direction that is not always uniquely defined. The only unambiguously defined quantity is the global (volumetric) consumption rate obtained by integrating the rate of reactant consumption over the entire combustion volume. However, using it to determine the FCS requires a proper identification of the flame surface area which introduces uncertainty in the results. Indeed, numerical simulations show that combustion properties depend significantly on the choices made in the determination of the FDS and FCS. In order to utilize these quantities in a meaningful way, their limitations are explored by providing a detailed comparison between predictions of numerical simulations and theoretical expressions obtained for weakly-stretched flames. The theory is based on the assumption that the flame is thin relative to the representative hydrodynamic length scale and in this asymptotic limit both, the FDS (commonly referred to as the flame speed) and the FCS, are uniquely and unambiguously defined. Two configurations are examined in this paper: (i) spherical flames, unsteady expanding as well as stationary, where the flow is unidirectional and (ii) steadily propagating cusp-like flames (resulting from the Darrieus-Landau instability) whose structures are spatially varying and where the flow through the flame is nonuniform. The presented comparison validates the accuracy of the asymptotic expressions for the dependence of the FDS and FCS on stretch for one-step chemistry, and demonstrates that the theoretical predictions remain qualitatively, and to a large extent quantitatively valid for detailed chemistry for both, lean and rich flames.

© 2019 The Combustion Institute. Published by Elsevier Inc. All rights reserved.

1. Introduction

The burning velocity, or propagation speed of a premixed flame is one of the most important characteristics of a combustible mixture and, evidently, one of great practical importance. The burning velocity of a planar flame propagating into a combustible mixture, say along the negative x -axis, which is commonly referred to as the *laminar flame speed*, is defined from the kinematic relation

$$S_L = -\frac{dx_f}{dt} \quad (1)$$

where $x = x_f(t)$ is an arbitrary location within the flame zone representing the *flame front*. The burning velocity of a planar flame can also be determined from the consumption rate of the deficient reactant: the fuel for lean mixtures and the oxidizer for rich mixtures. In a one-dimensional setting, the mass of combustible mixture flowing through the flame per unit area, per unit time, is constant, namely $\dot{m} = \rho_u S_L$ where ρ_u is the density of the unburned gas. If $\dot{\omega}_F$ is the mass rate at which fuel is consumed per unit volume, per unit time ($\dot{\omega}_F < 0$), the flame speed for lean conditions results from integrating the balance equation of the fuel mass fraction across the entire domain, from which

$$S_L = -\frac{1}{\rho_u Y_{F_u}} \int_{-\infty}^{\infty} \dot{\omega}_F dx, \quad (2)$$

* Corresponding author.

E-mail address: georgeg@lav.mavt.ethz.ch (G.K. Giannakopoulos).

Nomenclature

Acronyms

FCS	flame consumption speed
FDS	flame displacement speed

Greek Symbols

β	Zel'dovich number
δ	ratio of diffusion to hydrodynamic length scale
$\dot{\omega}$	reaction rate
$\dot{\omega}_i$	consumption rate of species i
κ	flame front curvature
Λ	reduced Damköhler number
λ	mixture thermal conductivity
μ	mixture viscosity
ν_i	stoichiometric coefficient of species i
Ω	global consumption rate
ϕ	equivalence ratio
ρ	density
σ	thermal expansion parameter
Θ	scaled temperature
$\xi_{1,2}$	transverse surface coordinates

Roman Symbols

$\mathbf{e}_1, \mathbf{e}_2$	transverse unit vectors
B	pre-exponential factor
L	Markstein length
R	gas constant
\dot{m}	mass flowrate
\dot{R}	propagation speed of spherical flame
l_e	deviation of Lewis number from unity
D	Damköhler number
K	flame stretch rate
V	volume of the domain
E	rate of strain tensor
n	unit normal to the flame
D_i	molecular diffusivity of species i
\hat{S}_d	density-weighted flame displacement speed
a, b	reaction orders
A_f	flame surface area
c_p	mixture specific heat
E	activation energy
$F(\mathbf{x}, t)$	function that determines the flame front
h_i	enthalpy function of species i
K_s	strain-rate experienced by flame
L	hydrodynamic length scale
l_f	diffusion length
l_T	(thermal) flame thickness
Le_i	Lewis number of species i
Le_{eff}	effective Lewis number
n	coordinate normal to the flame surface
p	pressure
Pr	Prandtl number
Q	total heat release
R	flame radius of spherical flame
s	normalized arc-length along the flame surface
S_c	flame consumption speed
S_d	flame displacement speed
S_f	laminar flame speed in asymptotic description
S_L	laminar flame speed
T	temperature
t	time
T_a	adiabatic flame temperature
T_u	unburnt gas temperature

U	propagation speed of steady cusp flame
W_i	molecular weight of species i
x_f	flame location
Y_i	mass-fraction of species i
Y_{i_b}	mass fraction of species i in burned mixture
Y_{i_u}	mass fraction of species i in unburned mixture
D_{th}	mixture thermal diffusivity
\mathcal{L}	asymptotic Markstein length
\mathcal{L}^b	burned Markstein length
\mathcal{L}_c	consumption Markstein length
\mathcal{L}_{cur}^*	curvature Markstein length at temperature T^*
\mathcal{L}_{str}^*	strain Markstein length at temperature T^*
M	Markstein number
M^b	burned Markstein number
M_c	consumption Markstein number

<i>Subscripts</i>	
c	consumption
f	flame
F, O	fuel, oxidizer
i, k	species index
u, b	unburned, burned

where Y_{F_u} is the fuel mass fraction in the fresh unburned mixture. For rich conditions, the mass fraction of the oxidizer in the fresh unburned mixture, Y_{O_u} , must be used instead. In either case, whether relying on the kinematic or consumption rate, the laminar flame speed is found to uniquely depend on the thermodynamic and transport properties of the combustible mixture and the description of the chemical kinetics. In general circumstances, when the flame is not planar and propagates against an arbitrary flow, the mass flux varies with distance through the flame and the definitions of flame speed and flame consumption speed become ambiguous.

The flame speed or flame consumption speed of multi-dimensional, time-dependent flames is expected to depend in general on the flame geometry, such as the local flame curvature and/or its surface gradient, and the underlying hydrodynamic strain. Such relations are not generally known, except for the case of weakly-stretched flames. Aspects of flow nonuniformities on flame dynamics have been examined by Karlovitz et al. [1], Klimov [2], Lewis and von Elbe [3], Buckmaster [4] and others. However, a systematic derivation by asymptotic methods led to the well-known linear relations between the flame speed and flame stretch [5,6], and between the flame consumption speed and flame stretch [7], where the stretch rate measures the overall surface deformation resulting from the motion of the flame and from the non-uniformities in the underlying flow field. These relations were derived using a multi-scale analysis that considers the thickness of the flame small compared to any other length scale L of the combustion field. If D_{th} is the thermal diffusivity of the mixture, the diffusion length $l_f = D_{th}/S_L$ is a characteristic length representing the flame thickness, and the underlying assumption is that $l_f/L = \delta \ll 1$. An analytical description of the flame structure is possible if one further assumes that the activation energy of the chemical reaction is large compared to the enthalpy of the fresh mixture, or the Zel'dovich number $\beta \gg 1$. The chemical activity is then restricted to a thin layer of thickness $\sim \beta^{-1} l_f$ embedded within the flame zone and the asymptotic theory is based on the dual limits $\delta \rightarrow 0$ and $\beta \rightarrow \infty$. When $\delta \rightarrow 0$, the flame consisting of the preheat and reaction zones shrinks to a surface determined by a smooth function $F(\mathbf{x}, t) = 0$, such that $F \leq 0$ correspond to the unburned/burned gas, respectively. The unit normal to the flame surface directed towards the burned gas, and the normal velocity of the flame surface measured with respect to a fixed coordinate

system, are respectively given by

$$\mathbf{n} = \frac{\nabla F}{|\nabla F|}, \quad V_f = -\frac{1}{|\nabla F|} \frac{\partial F}{\partial t}. \quad (3)$$

The flame speed, conventionally defined as the propagation relative to the incoming flow, is uniquely given by

$$S_f = -V_f + \mathbf{v} \cdot \mathbf{n}|_u \quad (4)$$

where \mathbf{v} is the gas velocity evaluated on the unburned side of the flame. As $\beta \rightarrow \infty$, the chemical reaction is negligible outside the reaction zone and the latter collapses to a sheet that coincides with the surface $F(\mathbf{x}, t) = 0$. The local consumption speed is then uniquely determined from

$$S_c = -\frac{1}{\rho_u (Y_{F_u} - Y_{F_b})} \int_{0^-}^{0^+} \dot{\omega}_F \, dn \quad (5)$$

where the integration is carried along n , the normal direction to the flame surface, unambiguously defined from (3). Here Y_{F_b} stands for the residual fuel on the burned side behind the flame front; i.e., at $n = 0^+$, a quantity that could vary along a corrugated flame. The local consumption of oxidizer is obtained similarly, using the mass fractions of the oxidizer Y_{O_u} and Y_{O_b} and its consumption rate $\dot{\omega}_O$. The definitions (4) and (5) are obvious generalizations of the kinematic and consumption speed relations (1) and (2).

Expressions for the flame speed and flame consumption speed result from the analytical solution describing the internal structure of the flame [5]. The expression for the flame speed takes the form

$$S_f = S_L - \mathcal{L} \mathbb{K}, \quad (6)$$

where \mathbb{K} is the flame stretch rate which combines the effects of surface curvature and hydrodynamic strain, and the proportionality coefficient \mathcal{L} , which accounts for the reactive and diffusive properties of the mixture and is known as the Markstein length in tribute to Markstein [8] who hypothesized a linear dependence of flame speed on curvature, albeit as a phenomenological constant. The asymptotic theory generalizes Markstein's proposition by including a dependence on hydrodynamic strain, absent in the Markstein model, and determines the coefficients \mathcal{L} from physical first principles. The expression for the consumption speed is of the form

$$S_c = S_L - \mathcal{L}_c \mathbb{K}, \quad (7)$$

and, by analogy, the coefficient \mathcal{L}_c will be referred to as the consumption Markstein length [7]. Both, the flame speed and flame consumption speed are *asymptotic concepts*, precisely and unambiguously defined when the flame zone shrinks to a surface. The stretch rate is then uniquely defined when referred to this surface and takes the same value when evaluated from the unburned or burned sides of the flame [9].

Experimental and numerical studies of flame dynamics that resolve the flame thickness face the difficulty of choosing an appropriate surface to represent the flame front. Typically a scalar iso-surface, such as temperature or species mass fraction, is selected arbitrarily with the flame displacement speed (FDS), similar to the flame speed, defined as the speed of this surface relative to the flow ahead¹. The subjective choice of the flame front leads to inconsistencies in the determination of the FDS, as demonstrated by Giannakopoulos et al. [10] for spherically-expanding flames. The flame consumption speed (FCS), used occasionally in numerical studies of flame dynamics, is typically computed by integrating the consumption rate of one of the reactants across the flame, similar

to (5), with the limits of integration specified approximately. This definition, however, may be appropriate for unidirectional flows, e.g., planar or spherical flames, where the normal to the flame is properly defined, but becomes ambiguous for corrugated flames because of significant variations in flow direction due to gas expansion. In addition, the result may become inaccurate when the flow does not tend to a uniform state behind the flame.

A property that does not suffer from ambiguity is the *global consumption rate*, obtained by integrating the rate of reactant consumption throughout the entire combustion volume \mathbb{V} . The global (volumetric) fuel consumption rate, defined from

$$\Omega = -\frac{1}{\rho_u (Y_{F,u} - Y_{F,b})} \int_{\mathbb{V}} \dot{\omega}_F \, dV \quad (8)$$

is a property that can be only determined numerically. When the flame is confined to a surface, as in the asymptotic theory, $\dot{\omega}_F$ is confined to the flame sheet and Ω is obtained by integrating the local consumption speed S_c over the entire flame surface area, namely

$$\Omega = \int_{A_f} S_c \, dA. \quad (9)$$

The FCS could then be obtained by normalizing Ω with the flame surface area A_f , namely

$$S_c = \Omega / A_f. \quad (10)$$

Using Eq. (10) to determine the FCS in numerical simulations with finite flame thickness, however, requires a proper identification of the flame surface, which introduces uncertainty in the results.

The objective of this work is to explore the limitations of using the flame displacement and consumption speeds by providing a detailed comparison between predictions of numerical simulations and the rigorous theoretical expressions. The uncertainty in determining the FDS, resulting from the selection of the iso-surface to represent the flame front, and the resulting wide spread in slope, or Markstein length, of the flame speed-flame stretch relation, ranging from positive slope when the isotherm is near the cold boundary of the flame to negative slope near the burned side, have been amply recognized in the literature [11–15]. Several studies have attempted to correlate their experimental or numerical data with the asymptotic expression (6) for the flame speed, failing to recognize that the Markstein length \mathcal{L} in this expression should only be used when the flame is treated as a hydrodynamic discontinuity. Others, have used experimental and/or numerical results to arbitrarily assign separate Markstein lengths for curvature and hydrodynamic strain. These issues have been unequivocally addressed in a recent study on outwardly propagating spherical flames [10] where expressions for the flame speed, and hence Marskein length, have been derived from the asymptotic theory at *any isotherm* within the flame zone. It was shown that separate Markstein lengths for strain and curvature exist when the isotherm selected to represent the flame surface is within the flame zone, but the two coincide when approaching the burned side temperature and tend to a constant value referred to as the “burned Markstein length”. The predicted flame speed and the corresponding Markstein lengths at various isotherms have been validated by numerical simulations with finite rate kinetics and detailed transport, for single-step and detailed chemistry descriptions. It was concluded that the proper choice of isotherm for the evaluation of the FDS must be selected sufficiently close to the burned side of the flame. Due to the diverging nature of the Markstein length when approaching the cold temperature, the FDS evaluated at an isotherm far from the maximum temperature may not characterize the combustion properties correctly and uniformly. The sensitivity of the FDS at different isotherms was recently examined by Thiesset et al. [16] for a corrugated flame

¹ The term “flame displacement speed” is used below when the surface representing the flame front is selected arbitrarily within the flame zone, contrary to “flame speed” referring to the unique surface determined in the asymptotic theory when $\delta \rightarrow 0$. Both, however, are defined from the kinematic relation (4).

interacting with a vortex, where it was experimentally shown that the Markstein length for curvature and strain are indeed different for isotherms close to the unburned side.

In this paper we show that the FCS for spherically-expanding flames does not suffer from the same difficulties as the FDS and, when properly determined, yields a unique result consistent with the asymptotic theory. This configuration, however, is exceptional because the flow is unidirectional and the normal to the flame front is at all times pointing in the radial direction. We have therefore investigated a second configuration, namely a steadily propagating cusp-like flame, which is spatially varying and where the flow through the flame is non-uniform. The orientation of the normal in this case varies significantly through the flame, particularly in highly-curved regions, an issue previously explored by van Oijen et al. [17] for turbulent expanding flames. The resulting FCS in this case exhibits peculiar behavior that appears to be inconsistent with theory. The evaluation of the FDS also suffers from the significant variations in curvature and strain across isotherms, which accentuate the difficulty in selecting a representative iso-surface to properly represent the flame. By elucidating these difficulties we propose ways to determine the FDS and FCS in a manner consistent with the asymptotic theory. Finally, we note that unlike planar flames where the FDS and FCS are both equal and represent the burning rate, the two quantities are different for general flames and measure different flame characteristics.

A similar definition to Eq. (10) for the FCS was given by Poinsot and Veynante [18]. For a spherically-expanding flame, they show by assuming the flame to be infinitesimally thin that $S_c = (\rho_b/\rho_u)\dot{R}$, where ρ_b is the density of the burned gas, $R(t)$ the radius of the flame front at time t , and \dot{R} the propagation velocity (the dot signifies differentiation with respect to time). They also noted that this relation must be corrected for effects due to the finite thickness of the flame and provided an estimate for this correction, later revisited by Bonhomme et al. [19], by assuming average properties for the variables affecting the flame structure. A rigorous account of the changes occurring inside the flame zone for spherical flames is shown in the Appendix to be consistent with the general asymptotic result (7) of weakly stretched flames. Moreover, it is demonstrated below that the two quantities, FDS and FCS, are not only distinct, but their difference exhibits a dependence on stretch with a well-defined slope. For spherically-expanding propane/air flames, for example, we show that in the range $0.8 \leq \phi \leq 2$, the slope of the dependence of the burned density-weighted FDS on stretch, or the associated Markstein length, is always negative while the consumption speed Markstein length becomes positive in sufficiently rich mixtures.

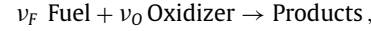
The distinction between the FDS and FCS has not been properly recognized in the literature. Considering spherically-expanding flames, the density-weighted FDS given by $(\rho_b/\rho_u)\dot{R}$ was evaluated experimentally in [19] and compared to the consumption speed S_c , defined as in Eq. (10) and obtained from numerical simulations, with the expectation that they represent the same quantity. Similarly, results for the dependence of the burned and unburned FDS on stretch were labeled in the figures of [20] as “consumption speed”. Another misconception resulted from the determination of the FCS from Eq. (10) which, as noted earlier, is highly sensitive to the selection of the flame radius $R(t)$ used to compute the surface area $A_f = 4\pi R^2$ which, when not carefully selected leads to inconsistent results about the dependence of the FCS on stretch [19,20]. It is shown below that the proper choice, consistent with the asymptotic theory, is the surface corresponding to the location where the reaction rate of the deficient component in the mixture (i.e., $\dot{\omega}_F$ for a lean mixture) reaches its maximum. We note that this location could differ significantly in numerical simulations when the chemistry is modeled by a one-step or a detailed mechanism, an issue that is further addressed below.

The paper is organized as follows: the asymptotic derivation of the FCS is presented in the next section; results on the displacement speed discussed in an earlier publication are summarized in Section 3; the methodology adopted in the numerical simulations is presented in Section 4; results of spherically-expanding flames and steady cusp-like flames are reported in Sections 5 and 6, and general conclusions are drawn in Section 7.

2. Flame consumption speed

In this section, we provide the main steps in the derivation on the consumption speed relation (7) which was first given by Bechtold and Matalon [7] with no details. The derivation relies on the hydrodynamic theory of premixed flames developed in [5,21] and for clarity we have adopted, to the extent possible, the same notation.

A global, one-step overall reaction



is assumed to describe the chemical activity between the fuel and oxidizer, proceeding at a rate

$$\dot{\omega} = \mathcal{B} \left(\frac{\rho Y_F}{W_F} \right)^a \left(\frac{\rho Y_O}{W_O} \right)^b e^{-E/\mathcal{R}T} \quad (11)$$

where Y_i , ν_i , W_i are the mass fraction, stoichiometric coefficient and molecular weight of species i (with $i = F, O$ denoting fuel and oxidizer), ρ and T are the density and temperature of the mixture, E and \mathcal{B} are the activation energy and pre-exponential factor of the chemical reaction, \mathcal{R} is the gas constant, and a , b are the reaction orders with respect to fuel and oxidizer. If the mass fractions of fuel and oxidizer in the fresh unburned mixture are Y_{F_u} and Y_{O_u} , the equivalence ratio $\phi = \nu Y_{F_u}/Y_{O_u}$ where $\nu = \nu_O W_O / \nu_F W_F$ is the ratio of the mass-weighted stoichiometric coefficients. Although the results below hold for the entire range - lean to rich conditions, it is convenient to focus on lean flames ($\phi < 1$), with the understanding that for rich flames the roles of fuel and oxidizer must be interchanged.

We non-dimensionalize lengths with respect to a hydrodynamic length scale L and velocities with respect to the laminar flame speed S_L , whilst time is scaled with respect to L/S_L . Temperature and density are scaled with respect to their values T_u and ρ_u in the fresh mixture and pressure is scaled with respect to $\rho_u S_L^2$. The specific heats are assumed equal and their common value, c_p , is taken as constant. The viscosity μ , thermal conductivity λ and molecular diffusivity D_i depend on temperature and are scaled with respect to their values in the fresh mixture. While the dependence of the transport coefficients on temperature remains arbitrary, their ratios consisting of the Prandtl, $Pr = \mu c_p / \lambda$, and Lewis, $Le_i = \lambda / c_p \rho D_i$, numbers are assumed constant, so that

$$\frac{\lambda}{\lambda_u} = \frac{\rho D_i}{\rho_u D_{i,u}} = \frac{\mu}{\mu_u} \equiv \tilde{\lambda}, \quad (12)$$

with $\tilde{\lambda} = \lambda(\tilde{T})$ and $\tilde{T} = T/T_u$ is the dimensionless temperature. Finally, we introduce a scaled dimensionless temperature $\Theta = (T - T_u)/(T_a - T_u)$, where $T_a = T_u + Q Y_{F_u} / c_p \nu_F W_F$ is the adiabatic flame temperature, with Q the total heat released during combustion.

In the following, when the same variables are used for dimensional and dimensionless quantities, the accent \sim on top of a variable identifies it as the dimensionless one; exceptions include the independent variables (time and spatial coordinates) and newly introduced symbols. The low Mach number governing equations in dimensionless form take the form

$$\frac{\partial \tilde{\rho}}{\partial t} + \nabla \cdot (\tilde{\rho} \tilde{\mathbf{v}}) = 0 \quad (13)$$

$$\tilde{\rho} \frac{D\tilde{\mathbf{v}}}{Dt} = -\nabla \tilde{p} + \delta \text{Pr} \nabla \cdot [\tilde{\lambda} (2\tilde{\mathbf{E}} - \frac{2}{3}(\nabla \cdot \tilde{\mathbf{v}})\mathbf{I})] \quad (14)$$

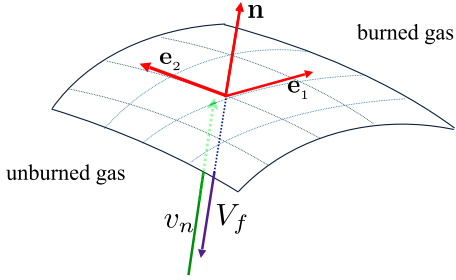


Fig. 1. Intrinsic curvilinear coordinates attached to the flame front.

$$\tilde{\rho} \frac{D\Theta}{Dt} - \delta \nabla \cdot (\tilde{\lambda} \nabla \Theta) = \delta^{-1} \tilde{\omega} \quad (15)$$

$$\tilde{\rho} \frac{DY_F}{Dt} - \delta Le_F^{-1} \nabla \cdot (\tilde{\lambda} \nabla Y_F) = -\delta^{-1} Y_{F_u} \tilde{\omega} \quad (16)$$

$$\tilde{\rho} \frac{DY_O}{Dt} - \delta Le_O^{-1} \nabla \cdot (\tilde{\lambda} \nabla Y_O) = -\phi Y_{O_u} \delta^{-1} \tilde{\omega} \quad (17)$$

$$\tilde{\rho} \{1 + (\sigma - 1)\Theta\} = 1 \quad (18)$$

where $\tilde{\mathbf{v}}$ is the velocity vector, $D/Dt = \partial/\partial t + \tilde{\mathbf{v}} \cdot \nabla$ is the convective derivative, and I is a unit tensor. The reaction rate is given by

$$\begin{aligned} \tilde{\omega} &= D \tilde{\rho}^{a+b} Y_F^a Y_O^b \exp \left\{ \frac{\beta \sigma (\Theta - 1)}{1 + (\sigma - 1)\Theta} \right\}, \\ D &= \frac{v_F W_F \rho_u^{a+b-1}}{Y_{F_u} W_F^a W_O^b S_L^2} \mathcal{D}_{th} \beta e^{-E/RT_a} \end{aligned} \quad (19)$$

where $\beta = E(T_a - T_u)/RT_a^2$ is the Zel'dovich number and $\sigma \equiv \rho_u/\rho_b$ the thermal expansion parameter.

We consider first the limit $\beta \gg 1$ (with δ retained finite), in which case the reaction rate is exponentially small and negligible, except in the region where $\Theta - 1 = \mathcal{O}(\beta^{-1})$. The extent of the reaction zone is therefore the region where the temperature remains sufficiently close to the adiabatic flame temperature. Since in the limit $\beta \rightarrow \infty$ the reaction zone shrinks to the surface $F(\mathbf{x}, t) = 0$, it is convenient to adopt a curvilinear coordinate system (n, ξ_1, ξ_2) attached to the reaction sheet, with n measured along the normal \mathbf{n} to the sheet (pointing towards the burned gas) and ξ_1, ξ_2 transverse surface coordinates along $\mathbf{e}_1, \mathbf{e}_2$, as illustrated in Fig. 1.

For self-consistency, the asymptotic treatment requires simultaneously considering a near-stoichiometric limit, for which $Y_{O_u} - \nu Y_{F_u} = \mathcal{O}(\beta^{-1})$, or $1 - \phi = \mathcal{O}(\beta^{-1})$, and a near-equidiffusion formulation, whereby $Le_i^{-1} = 1 - \beta^{-1} le_i$ with le_i being the deviation of the Lewis numbers from unity. It is thus convenient to introduce

$$\theta \sim \begin{cases} e^\eta + \delta \left\{ \frac{\gamma_1 \tilde{\kappa}}{\sigma} ((1-\eta)e^\eta - 1) - \frac{\beta}{2} (Le_{eff} - 1) \gamma_2 \tilde{\kappa} \eta e^\eta + \chi_2(\eta) \right\} & \text{for } \eta < 0 \\ 1 & \text{for } \eta > 0 \end{cases} \quad (25)$$

the enthalpy functions, h_F and h_O , defined from the relations

$$\Theta + Y_F/Y_{F_u} = 1 + \beta^{-1} h_F + \dots, \quad \Theta + Y_O/Y_{O_u} = 1 + \beta^{-1} h_O + \dots$$

in lieu of the mass fractions, along with the expansion $\Theta \sim \theta_0 + \beta^{-1} \theta_1 + \dots$. Being the deficient component in the mixture, the fuel is totally consumed such that

$$Y_F = 0, \quad \Theta = 1 + \beta^{-1} h_F, \quad Y_O = \beta^{-1} Y_{O_u} (h_O - h_F)$$

in the burned gas region ($n > 0$). The flame temperature and the amount of oxidizer that leaks through the reaction zone are then given by $\Theta_f = 1 + \beta^{-1} h_{F_b}$ and $Y_{O_b} = \beta^{-1} Y_{O_u} (h_{O_b} - h_{F_b})$, where the subscript b denotes values at $n = 0^+$. Removing the subscript in θ_0 to simplify the notation, the equations on either side of the reaction sheet reduce to

$$\begin{aligned} \tilde{\rho} \frac{D\theta}{Dt} - \delta \nabla \cdot (\tilde{\lambda} \nabla \theta) &= 0 & \text{for } n < 0 \\ \theta &= 1 & \text{for } n > 0 \end{aligned} \quad (20)$$

$$\tilde{\rho} \frac{Dh_i}{Dt} - \delta \nabla \cdot (\tilde{\lambda} \nabla h_i) = \delta I e_i \nabla \cdot (\tilde{\lambda} \nabla \theta), \quad i = F, O \quad \text{for } n \leq 0. \quad (21)$$

Introducing the stretching transformation $n = \hat{\eta}/\beta$ and the expansions $\theta = 1 + \beta^{-1} \hat{\theta} + \dots$, $h_i = h_{i_b} + \beta^{-1} \hat{h}_i + \dots$, the energy equation in the reaction zone simplifies, to leading order, to

$$-\tilde{\lambda}_b \delta^2 \frac{\partial^2 \hat{\theta}}{\partial \hat{\eta}^2} = \underbrace{\Lambda (h_{F_b} - \hat{\theta})^a (h_{O_b} - \hat{\theta})^b e^{\hat{\theta}}}_{\hat{\omega}_0}, \quad (22)$$

with the reduced Damköhler number $\Lambda = \tilde{\rho}_b^{a+b} Y_{F_u}^a Y_{O_u}^b \beta^{-(a+b+1)} \mathbb{D} = \mathcal{O}(1)$. Note that to ensure a balance between diffusion and reaction, the reaction rate has been expanded in the form $\tilde{\omega} = \beta \tilde{\omega}_0 + \tilde{\omega}_1 + \dots$, with the leading term retained in (22). A first integration of (22) provides the jump conditions across the reaction sheet that are needed to solve (20) and (21).

Since the reaction rate is exponentially small and therefore negligible on either side of the reaction sheet, the consumption speed (in dimensionless form) is determined from

$$\tilde{\xi}_c = \delta^{-1} \int_{-\infty}^{\infty} \tilde{\omega}_0 d\hat{\eta} = -\delta \tilde{\lambda}_b \frac{\partial \hat{\theta}}{\partial \hat{\eta}} \Big|_{\hat{\eta}=-\infty}^{+\infty},$$

where use has been made of (22). Matching the slopes with their counterparts as $\hat{\eta} \rightarrow \pm\infty$, then using the requirement $\partial \hat{\theta}/\partial \hat{\eta} \rightarrow 0$ as $\hat{\eta} \rightarrow \infty$, yields

$$\tilde{\xi}_c = \delta \tilde{\lambda}_b \frac{\partial \theta}{\partial n} \Big|_{n=0^-}. \quad (23)$$

The determination of the temperature gradient $\partial \theta / \partial n$ at the upstream edge of the reaction zone or, equivalently (due to the inherent symmetry) the mass flux of fuel that ensures complete combustion is, in general, a nontrivial task that can be carried out analytically for thin flames, as discussed in [5,21].

The internal structure of the flame, for $\delta \ll 1$, is examined by introducing the stretched coordinate

$$\eta = \int_0^{n/\delta} \frac{dn'}{\tilde{\lambda}(n')} \quad (24)$$

and carrying out the solution to $\mathcal{O}(\delta)$ in order to account for the variations occurring inside the thin, but finite flame zone. One finds

$$\theta \sim \begin{cases} e^\eta + \delta \left\{ \frac{\gamma_1 \tilde{\kappa}}{\sigma} ((1-\eta)e^\eta - 1) - \frac{\beta}{2} (Le_{eff} - 1) \gamma_2 \tilde{\kappa} \eta e^\eta + \chi_2(\eta) \right\} & \text{for } \eta < 0 \\ 1 & \text{for } \eta > 0 \end{cases} \quad (25)$$

where

$$\chi_2(\eta) = \int_\eta^0 \left(\tilde{\kappa} I(\eta') - \tilde{\kappa} J(\eta') + \tilde{\lambda} \tilde{\kappa} \right) (e^{\eta'} - e^\eta) d\eta'$$

$$I(\eta) = - \int_{\tau(\eta)}^\sigma \frac{\tilde{\lambda}(x)}{x-1} dx, \quad J(\eta) = - \int_{\tau(\eta)}^\sigma \frac{\tilde{\lambda}(x)}{x(x-1)} dx,$$

with $\tau(\eta) = 1 + (\sigma - 1)e^\eta$. Here Le_{eff} is a weighted average of the individual Lewis numbers defined below, $\tilde{\kappa} = \tilde{\kappa} + \tilde{K}_s$ is the dimensionless stretch rate (scaled by S_L/L) with $\tilde{\kappa} = -\nabla \cdot \mathbf{n}$ the curvature

of the flame surface and $\tilde{K}_s = -\mathbf{n} \cdot \tilde{\mathbf{E}} \cdot \mathbf{n}$ the rate of strain experienced by the flame, and the coefficients γ_1, γ_2 are given by

$$\gamma_1 = \frac{\sigma}{\sigma-1} \int_1^\sigma \frac{\tilde{\lambda}(x)}{x} dx, \quad \gamma_2 = \frac{1}{\sigma-1} \int_1^\sigma \frac{\tilde{\lambda}(x)}{x} \ln\left(\frac{\sigma-1}{x-1}\right) dx.$$

Evaluating $\partial\theta/\partial n$ at $n = 0^-$, then substituting in (23), one finds

$$\tilde{S}_c = 1 - \frac{\beta}{2} (\text{Le}_{\text{eff}} - 1) \delta \gamma_2 \tilde{\mathbb{K}}$$

which, when recast in dimensional form, yields Eq. (7) for the flame consumption speed with \mathbb{K} the dimensional stretch rate and

$$\mathcal{L}_c = \left\{ \frac{1}{2} \frac{\beta(\text{Le}_{\text{eff}} - 1)}{\sigma-1} \int_1^\sigma \frac{\tilde{\lambda}(x)}{x} \ln\left(\frac{\sigma-1}{x-1}\right) dx \right\} l_f. \quad (26)$$

The effective Lewis number is found to be

$$\text{Le}_{\text{eff}} = \frac{\text{Le}_0 + \text{Le}_F \mathcal{A}}{1 + \mathcal{A}}, \quad \mathcal{A} = \frac{\mathcal{G}(a, b; \varphi)}{b \mathcal{G}(a, b-1; \varphi)} - 1, \quad (27)$$

where the coefficient \mathcal{A} depends on the stoichiometric condition, and the function

$$\mathcal{G}(a, b; \varphi) \stackrel{\text{def}}{=} \int_0^\infty \varsigma^a (\varsigma + \varphi)^b e^{-\varsigma} d\varsigma$$

depends on the reaction orders, a and b , and on $\varphi = \beta |1 - \phi|$ that measures the departure from stoichiometry. When $\varphi = 0$, the function \mathcal{G} can be expressed in terms of the gamma function, $\mathcal{G} = \Gamma(a+b+1)$, such that $\mathcal{A} = a/b$. As φ increases, the Lewis number of the fuel (here the deficient component) becomes more heavily weighted and for conditions sufficiently remote from stoichiometry $\text{Le}_{\text{eff}} \approx \text{Le}_F$. For rich conditions, it is the oxidizer which is more heavily weighted, in which case $\text{Le}_{\text{eff}} \approx \text{Le}_0$. For unitary reaction orders $a=b=1$, the coefficient $\mathcal{A} = 1 + \varphi$. Finally, we note that the consumption speed, $S_c = S_c(\xi_1, \xi_2, t)$ is a local property that measures the instantaneous rate of fuel consumption across the reaction zone at a given point along the reaction sheet.

The enthalpy functions h_F and h_O and, in particular, their values at the reaction sheet

$$h_{F_b} = -\delta \text{le}_F \gamma_2 \tilde{\mathbb{K}}, \quad h_{O_b} = -\delta \text{le}_0 \gamma_2 \tilde{\mathbb{K}},$$

determine the flame temperature and the excess reactant that leaks through the reaction zone, respectively. For a lean mixture, the flame temperature (in dimensional form) is given by

$$T_f = T_a - T_u \left\{ (\text{Le}_F - 1) \int_1^\sigma \frac{\tilde{\lambda}(x)}{x} \ln\left(\frac{\sigma-1}{x-1}\right) dx \right\} \frac{l_f \mathbb{K}}{S_L} \quad (28)$$

and the mass fraction of oxidizer leaking through the flame is

$$Y_{O_b} = Y_{O_u} \frac{\text{Le}_F - \text{Le}_0}{\sigma-1} \left\{ \int_1^\sigma \frac{\tilde{\lambda}(x)}{x} \ln\left(\frac{\sigma-1}{x-1}\right) dx \right\} \frac{l_f \mathbb{K}}{S_L}. \quad (29)$$

Similar expressions can be written for rich mixtures by simply interchanging the role of the reactants. We note that unlike the FCS and the FDS discussed below that depend on the effective Lewis number Le_{eff} of the mixture, the flame temperature depends on the Lewis number of the deficient component in the mixture, i.e., the fuel in lean and the oxidizer in rich mixtures, whilst the extent to which the reactants leak through the flame depends on the difference of the two.

3. Flame displacement speed

The asymptotic expression (6) for the flame speed was obtained by considering the limit $\delta \rightarrow 0$, namely when the entire flame is confined to a surface, with the corresponding Markstein length [21,22] given by

$$\mathcal{L} = \left\{ \frac{\sigma}{\sigma-1} \int_1^\sigma \frac{\tilde{\lambda}(x)}{x} dx + \frac{1}{2} \frac{\beta(\text{Le}_{\text{eff}} - 1)}{\sigma-1} \int_1^\sigma \frac{\tilde{\lambda}(x)}{x} \ln\left(\frac{\sigma-1}{x-1}\right) dx \right\} l_f = \alpha l_f. \quad (30)$$

In numerical simulations (and in experimental measurements) that resolve the flame thickness, the flame displacement speed (FDS) is defined as the speed of a scalar iso-surface, arbitrarily selected to represent the flame surface. The Markstein length \mathcal{L} resulting from the asymptotic derivation does not correspond to any specific iso-surface within the flame zone and should be used only when the flame is treated as a hydrodynamic discontinuity.

It has been recently demonstrated [10] that the asymptotic theory yields expressions for the displacement speed of various isotherms within the flame zone, which are substantially different from Eq. (6). Since significant variations in density occur from the unburned side of the flame up to the iso-surface corresponding to $T = T^*$, a density-weighted displacement speed is used instead, defined as

$$\widehat{S}_d^* = \frac{\rho^*}{\rho_u} S_d^*,$$

where ρ^* is the density along the selected isotherm; the subscript d is used to distinguish the FDS from the asymptotic flame speed S_f . The result²

$$\begin{aligned} \widehat{S}_d^* &= S_L - \underbrace{\left(\alpha - \int_1^{\tilde{T}^*} \frac{\tilde{\lambda}(x)}{x} dx - \int_{\tilde{T}^*}^\sigma \frac{\tilde{\lambda}(x)}{x-1} dx \right) l_f K_s}_{\mathcal{L}_{\text{str}}^*} \\ &\quad - \underbrace{\left(\alpha - \int_1^{\tilde{T}^*} \frac{\tilde{\lambda}(x)}{x} dx \right) l_f \kappa S_L}_{\mathcal{L}_{\text{cur}}^*} \end{aligned} \quad (31)$$

indicates the existence of two Markstein lengths, one associated with strain, $\mathcal{L}_{\text{str}}^*$, and the other with curvature, $\mathcal{L}_{\text{cur}}^*$, as first noted by Bechtold and Matalon [7]. On the burned side of the flame, the strain and curvature Markstein lengths are equal and a single proportionality coefficient emerges - the “burned Markstein length” $\mathcal{L}^b = \mathcal{L}_{\text{cur}}^* = \mathcal{L}_{\text{str}}^*$, given by

$$\begin{aligned} \mathcal{L}^b &= \left\{ \alpha - \int_1^\sigma \frac{\tilde{\lambda}(x)}{x} dx \right\} l_f \\ &= \left\{ \frac{1}{\sigma-1} \int_1^\sigma \frac{\tilde{\lambda}(x)}{x} dx + \frac{1}{2} \frac{\beta(\text{Le}_{\text{eff}} - 1)}{\sigma-1} \int_1^\sigma \frac{\tilde{\lambda}(x)}{x} \ln\left(\frac{\sigma-1}{x-1}\right) dx \right\} l_f. \end{aligned} \quad (32)$$

Elsewhere, the two Markstein lengths are different from each other with $\mathcal{L}_{\text{cur}}^* = \alpha$ and $\mathcal{L}_{\text{str}}^* \rightarrow -\infty$ as $\tilde{T}^* \rightarrow 1$. The singular nature of Markstein length when $\tilde{T}^* \rightarrow 1$ compared to its asymptotic approach to \mathcal{L}^b when $\tilde{T}^* \rightarrow \sigma$, implies that the proper isotherm for the evaluation of the FDS, that is well-conditioned and less prone to numerical uncertainties, must be selected sufficiently close to the burned side of the flame. Only when evaluated at the burned side of the flame does the density-weighted FDS, or equivalently the asymptotic flame speed measured relative to the burned gas \dot{S}_f , exhibit a linear dependence on stretch, of the form

$$\widehat{S}_d^b = \dot{S}_f^b / \sigma = S_L - \mathcal{L}^b \mathbb{K}. \quad (33)$$

One exception is the spherically-expanding flame, where a linear dependence on stretch results at any reference location within the flame zone, because curvature and strain are both inversely proportional to the flame radius R and thus, proportional to each other and to the total stretch rate \mathbb{K} , as discussed in [10].

² For consistency, only the leading term in the expression for the temperature needs to be retained, so that $1 < \tilde{T}^* < \sigma$.

Table 1

Parameters corresponding to propane-air mixtures at 298 K and 1 atm.

ϕ	B (cm ³ ·s/mol)	T_b/T_u	ρ_u/ρ_b	S_L (cm/s)	l_f (mm)	l_T (mm)	β
0.8	6.2e15	6.94	7.16	28.78	0.0721	0.393	8.42
1.0	5.4e15	8.02	8.34	40.35	0.0507	0.317	7.43
1.2	4.5e15	7.79	8.1	40.91	0.0493	0.296	7.59
1.4	2.0e15	7.58	7.88	27.74	0.0717	0.416	7.76
2.0	7.5e13	7.04	7.31	3.91	0.4899	2.615	8.28

As a final comment, we note that the difference between the burned and consumption Markstein lengths, given by

$$\mathcal{L}^b - \mathcal{L}_c = \left\{ \frac{1}{\sigma - 1} \int_1^\sigma \frac{\tilde{\lambda}(x)}{x} dx \right\} l_f, \quad (34)$$

is independent of the Lewis and Zel'dovich numbers (apart from minor variations in l_f) and is always positive. Consequently, the difference

$$S_c - \tilde{S}_d^b = (\mathcal{L}^b - \mathcal{L}_c) \mathbb{K} \quad (35)$$

is a linear function of stretch with a positive slope that is practically independent of the mixture composition, except for small variations in the heat of combustion that affects the thermal expansion coefficient σ and the functional dependence of $\tilde{\lambda}$ on temperature.

4. Flame configurations and numerical methodology

Two configurations will be examined in this paper. The first is a spherically-expanding flame where, following ignition, a spherical flame propagates outwards consuming the fresh mixture and leaving behind a motionless pocket of burned products. With the flame surface represented by $r = R(t)$, the propagation speed $V_f = \dot{R}$ and, since the burned gas is at rest, V_f is also equal to the flame speed relative to the burned gas S_f^b . The flow induced by thermal expansion in the unburned gas ahead of the flame varies radially and tends to zero at large distances. The second configuration is a two-dimensional steadily propagating cusp-like flame resulting from the nonlinear consequences of the Darrieus-Landau (DL) instability investigated numerically in [23–25]. The flame propagates as a whole at a constant speed, significantly larger than the laminar flame speed S_L . The flow field across the flame is highly nonuniform, with the motion induced in the unburned gas directed towards the highly rounded cusp to maintain its structure.

Premixed propane/air mixtures with equivalence ratios ϕ ranging from 0.8 to 2 are considered at $T_u = 298$ K and pressure $p = 1$ atm. The chemistry is described by a global single-step reaction and is assumed to proceed at a rate given by Eq. (11) with reaction orders $a=b=1$, as proposed by Kim et al. [26]. The activation energy is kept fixed at $E = 40.2$ kcal/mol. The pre-exponential factor B is adjusted for every ϕ to match the value of the laminar flame speed S_L obtained independently from one-dimensional laminar flame calculations using the detailed reaction mechanism proposed by Qin et al. [27]. The solution of the planar adiabatic flame obtained by PREMIX [28] provided the laminar flame speed S_L , the burned gas temperature T_b , the products composition, and an estimate of the (thermal) flame thickness l_T defined from $l_T = (T_b - T_u)/\max(dT/dx)$. Note that l_T differs from the diffusion length l_f used as reference in the asymptotic theory and both differ from the “real” thickness of the flame that extends from $0.01T_u$ to $0.99T_b$ and corresponds approximately to $7-9l_f$ or $1.5-3l_T$. The values of the aforementioned parameters are listed in Table 1.

Comparison of numerical simulations with the corresponding asymptotic results, requires the determination of the Markstein lengths and, therefore, specification of β , σ , l_f and Le_{eff} . The effective Lewis number Le_{eff} is obtained from Eq. (27) with the limiting

Lewis numbers taken as $Le_F = 1.81$ and $Le_O = 0.901$, as discussed in [10]; β is based on the overall activation energy E , and σ and l_f are taken from Table 1. These parameters and the predicted values of the various Markstein lengths (the asymptotic Markstein length \mathcal{L} , the burned Markstein length \mathcal{L}^b and the consumption Markstein length \mathcal{L}_c for constant transport coefficients, i.e., $\tilde{\lambda} = 1$), are given in Table 2 for $0.8 \leq \phi \leq 2$. For completeness, we also provide values of the asymptotic $\mathcal{M} \equiv \mathcal{L}/l_f$, burned $\mathcal{M}^b \equiv \mathcal{L}^b/l_f$ and consumption $\mathcal{M}_c \equiv \mathcal{L}_c/l_f$ Markstein numbers.

The numerical simulations are based on the low Mach-number form of mass, momentum, energy and species conservation equations, which account for density variations due to the heat release but filter out acoustic disturbances. The flame thickness l_T and the laminar flame speed S_L are used as the reference length and velocity scales, and the state of the fresh mixture as reference for all state variables. The gaseous mixture is assumed to be an ideal gas, and species diffusion is based on Curtiss-Hirschfelder expression with diffusivities given by a mixture-average formulation. The equations are discretized in space using the spectral element method [29,30] in computational domains that are split into conforming quadrilateral elements. The geometry and the solutions are expressed as N^{th} -order tensor product Lagrange polynomials, based on the Gauss-Lobatto-Legendre quadrature points, and the discretized equations are integrated in time using the highly-efficient parallel code nek5000 [31] which uses a high-order splitting scheme [32]. A third-order semi-explicit integration scheme is used for the continuity and momentum equations, while the energy and species equations are integrated implicitly without further splitting using CVODE [33]. Further details of the mathematical formulation, numerical method as well as a validation of the approach along with numerical benchmarking tests can be found in [32,34]. CHEMKIN transport and thermo-chemistry libraries [35,36] are employed for the evaluation of the transport and thermodynamic properties.

In numerical simulations, the FDS associated with a given isotherm is determined either directly from the kinematic relation (4), with $F(\mathbf{x}, t) \equiv T(\mathbf{x}, t) - T^*$, or from the energy conservation equation, as discussed in [10]. The FCS is evaluated based on Eq. (5) with the integration performed over the region where the reaction rate is finite and not negligible. Some ambiguity exists when the direction of the normal varies significantly throughout the reaction zone, an issue that will be further discussed below. The evaluation of flame stretch, on the other hand, is more problematic because it is not evident a priori which surface should be used to represent the flame front. Since flame stretch is an asymptotic concept, the choice should rely on insight from the asymptotic derivation. Flame stretch is defined as the fractional rate of change in area of a Lagrangian element of the flame surface [1,37], and a direct computation of the time derivative of an area element deformed by the underlying flow yields [9]

$$\mathbb{K} = -V_f \kappa - \mathbf{n} \cdot \nabla \times (\mathbf{v} \times \mathbf{n}) \stackrel{\text{or}}{=} -V_f \kappa + \nabla_s \cdot \mathbf{v}_s \quad (36)$$

where \mathbf{v}_s is the component of the velocity vector tangent to the flame surface and ∇_s is the surface gradient³. This expression clearly illustrates the two mechanisms by which the flame surface can be stretched; the first is the *surface dilatation* resulting from the motion of a curved segment of the flame and the second is the *surface extension/compression* resulting from the velocity gradient along the flame surface. Eq. (36) provides a unique value for \mathbb{K} , regardless of whether it is evaluated on the unburned or burned side of the flame front. It is a convenient formula for evaluating the stretch rate in circumstances when the velocity gradient along the

³ The surface gradient ∇_s consists of derivatives in the transverse directions ξ_1 and ξ_2 weighted appropriately by the scale factors of the curvilinear coordinate system; see Appendix A in [21].

Table 2

The theoretically-predicted asymptotic Markstein length \mathcal{L} , burned Markstein length \mathcal{L}^b , consumption Markstein length \mathcal{L}_c and the corresponding Markstein numbers (scaled by l_f), for propane-air mixtures at 298K and 1atm.

ϕ	σ	l_f (mm)	l_T (mm)	Le_{eff}	β	\mathcal{L} (mm)	\mathcal{M}	\mathcal{L}^b (mm)	\mathcal{M}^b	\mathcal{L}_c (mm)	\mathcal{M}_c
0.8	7.16	0.0721	0.393	1.59	8.42	0.2563	3.552	0.1144	1.583	0.091	1.262
1.0	8.34	0.0507	0.317	1.36	7.43	0.1545	3.040	0.0470	0.919	0.032	0.631
1.2	8.1	0.0493	0.296	1.16	7.59	0.1321	2.679	0.0290	0.587	0.014	0.284
1.4	7.88	0.0717	0.416	1.08	7.76	0.1804	2.514	0.0324	0.450	0.011	0.153
2.0	7.31	0.4899	2.615	0.989	8.28	1.1180	2.282	0.1440	0.293	-0.011	-0.022

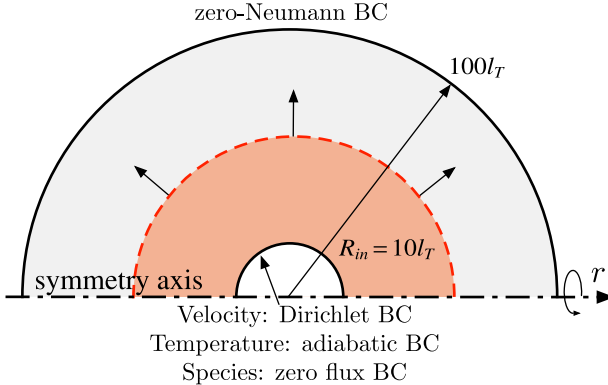


Fig. 2. Schematic of the computational domain and boundary conditions (BC) used in the numerical simulation of a spherically-expanding flame. The darker/lighter shaded regions correspond to the burned/unburned gas, respectively.

flame surface is obvious, such as spherical flames where the flow is radial and the tangential component of the velocity is identically zero, or flat flames in stagnation-point flow where the transverse velocity gradient is equal to a constant strain rate. It has been used also in studies based on the hydrodynamic theory where the flame is confined to a well-defined surface [38].

As noted earlier, the stretch rate can be also expressed as a combination of curvature and strain in the form $\mathbb{K} = S_f \kappa + K_s$, which can be verified by expanding Eq. (36) and recognizing that

$$\mathbb{K} = \underbrace{(\mathbf{v} \cdot \mathbf{n} - V_f) \kappa}_{S_f} + \underbrace{(-(\mathbf{v} \cdot \mathbf{n}) \kappa - \mathbf{n} \cdot \nabla \times (\mathbf{v} \times \mathbf{n}) - \nabla \cdot \mathbf{v})}_{K_s}. \quad (37)$$

The two formulas give the same value of \mathbb{K} only when the divergence of the velocity is identically zero, consistent with the asymptotic viewpoint that the flame is a surface separating two regions of constant but different densities. Equation (37) is often used in computational studies because the strain rate \mathbf{E} is already implemented in most codes, but the resulting stretch rate \mathbb{K} is not uniquely determined because the divergence of the velocity in the expression for the strain rate K_s does not vanish at any selected location within the flame region. To remain consistent with the theory, the constraint $\nabla \cdot \mathbf{v}$ must be imposed when evaluating the strain rate K_s as further elaborated below. It should be also noted that, unlike (36), Eq. (37) does not genuinely separate the influences of curvature and strain on stretch since K_s also depends on curvature. For a spherically-expanding flame, for example, the strain rate experienced by the flame, $K_s = 2(\sigma - 1)S_f/R$, is proportional to the flame front curvature $\kappa = 2/R$, and the total stretch rate $\mathbb{K} = 2\dot{R}/R = \sigma S_f \kappa$ is also proportional to curvature.

5. Spherically expanding flames

The computational domain for the simulation of the spherically-expanding flames shown schematically in Fig. 2 is discretized by 200 and 40 spectral elements in the radial and

azimuthal directions, respectively. In combination with the ninth-order interpolating polynomials, the thermal flame thickness l_T is discretized by approximately 20 grid points. The outer radius of the computational mesh, $R_{out} = 100l_T$, is smaller than the critical radius beyond which such flames may be subject to the hydrodynamic instability [39,40]; thermo-diffusive instabilities are practically inactive for the mixtures considered here. For all variables, axisymmetric boundary conditions are applied along the symmetry axis and zero-Neumann boundary conditions along the outer boundary. At the inner spherical boundary, $R_{in} = 10l_T$, Dirichlet BC are imposed for the velocity ($\mathbf{v} = 0$), adiabatic BC for the temperature and zero flux for the species. A hot kernel of burned gases of radius $r = 15l_T$ is selected as the initial condition, with the states of the burned products and fresh reactants connected by a hyperbolic tangent profile. This configuration properly simulates a three-dimensional outwardly-propagating spherical flame.

Instantaneous profiles of the temperature and rate of volume dilatation across the flame zone for a mixture with equivalence ratio $\phi = 2$ are shown in Fig. 3(a). The flame zone approximately spans the region where the rate of volume dilatation resulting from gas expansion is nonzero, or the temperature rises from $\tilde{T} = 1$ to $\tilde{T} = 7.04$, namely $33 < r/l_T < 36$. Note that the velocity divergence reaches its maximum value near the location of maximum temperature gradient and vanishes on both sides of the flame. Also plotted in this figure is the temperature profile (dashed blue line) obtained from (25) using the data reported in Tables 1 and 2, with $\tilde{\lambda} = 1$. The comparison shows that the two-term asymptotic expression approximates the numerical solution reasonably well. The main difference is the thin reaction zone near the point of maximum heat release rate ($T \approx 6$) which, due to the large activation energy assumption adopted in the theory is confined to a sheet that generates a discontinuous temperature gradient.

In Fig. 3(b), we show the deviation of the stretch rate evaluated from Eq. (37) along surfaces corresponding to different isotherms within the flame zone from its exact asymptotic value. With $r = R(t)$ representing the flame front, the stretch rate computed from Eq. (36) is uniquely determined by $\mathbb{K} = 2\dot{R}/R$ and can be evaluated numerically from this expression with sufficient accuracy, irrespective of how precisely the flame radius R is defined. When using Eq. (37), however, the computed stretch rate is found to vary throughout the flame zone and is equal to the unique asymptotic value only at the cold and hot boundaries. The discrepancy, shown by the blue curve in the figure (in dimensionless form), is exactly equal to the rate of volume dilatation (red curve) such that, when imposing the constraint $\nabla \cdot \mathbf{v} = 0$ in evaluating K_s the correct stretch rate is recovered.

Figure 4 compares the density-weighted FDS and FCS extracted from the simulations (filled symbols) with the asymptotic predictions for $\tilde{\lambda} = 1$ (solid lines) for varying stretch rates and equivalence ratios. The FDS here corresponds to isotherms very close to the burned side of the flame which, as noted earlier, are the appropriate reference locations that describe the overall flame propagation and its dependence on stretch. The FCS is determined from the direct definition (5). Due to the non-dimensionalization adopted in

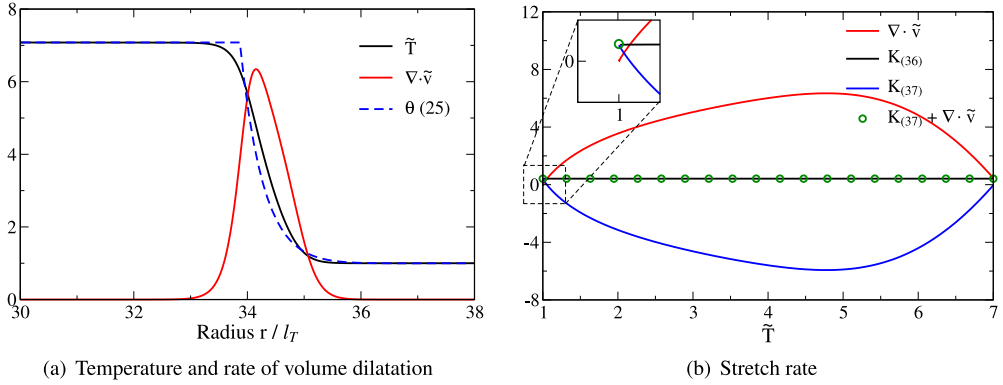
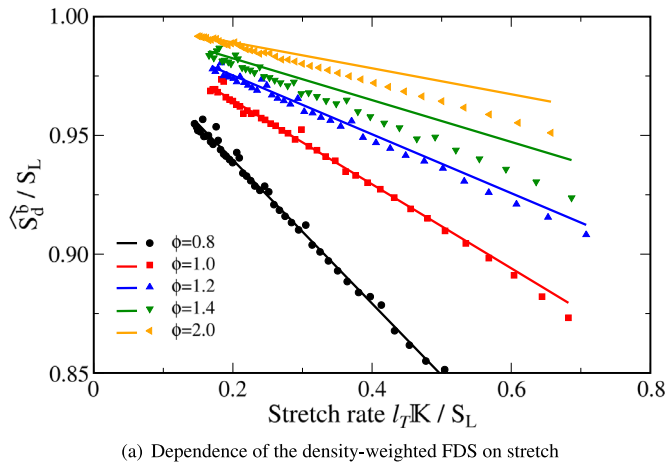


Fig. 3. (a) Theoretical (dashed curve) and numerical (solid curve) profiles of temperature and rate of volume dilatation across the flame zone and, (b) stretch rate at different isotherms within the flame zone evaluated from its exact relation (36) and alternatively from (37) with/without applying the divergence-free constraint. The results correspond to a propane/air spherically-expanding flame of equivalence ratio $\phi = 2$ at time $t = 2.75l_T/S_L$.



(a) Dependence of the density-weighted FDS on stretch

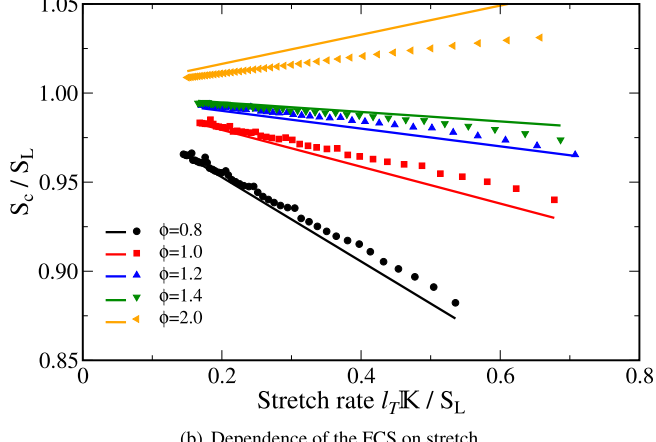


Fig. 4. Comparison of the dependence of the FDS and FCS on stretch between theoretical predictions (solid curves, assuming $\tilde{\lambda} = 1$) and results of numerical simulations (symbols) for different values of equivalence ratio ϕ .

the figure, which is based on the reference length scale l_T used in the simulations, the slopes of the theoretical curves corresponding to \mathcal{L}^b/l_T and \mathcal{L}_c/l_T differ slightly from the conventional Markstein numbers which are scaled by the diffusion length l_f . A very good agreement is observed between numerical simulations and theory: the FDS and FCS in this weakly stretched regime depend linearly on stretch, the slopes traced by the numerical data is well predicted by the asymptotic expressions (33) and (7), and both extrapolate to the laminar flame speed S_L when $\mathbb{K} \rightarrow 0$. We note that the

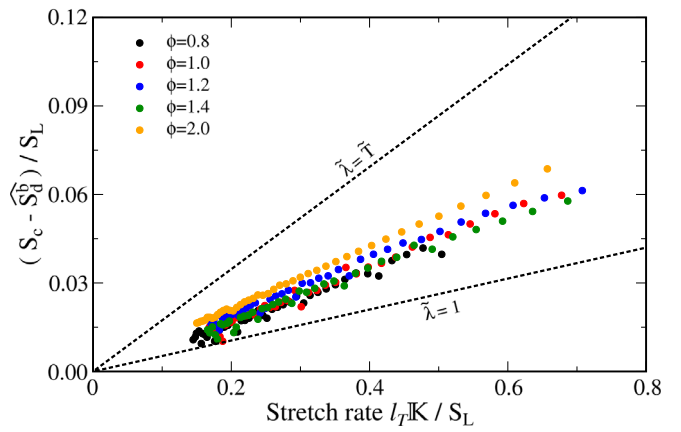


Fig. 5. The dependence of $(S_c - \hat{S}_d^b)/S_L$ of outwardly propagating spherical flames on the stretch rate $l_T \mathbb{K} / S_L$ for different values of equivalence ratio ϕ . The filled symbols correspond to the numerical data and the two dashed lines are based on the theoretical expression (35) for constant ($\tilde{\lambda} = 1$) and variable ($\tilde{\lambda} = \tilde{T}$) transport for $\sigma = 7.76$ (see text).

consumption Markstein length \mathcal{L}_c differs from the burned Markstein length \mathcal{L}^b and, while the latter has the same sign for all the mixtures considered, even for $\phi = 2$ corresponding to Le_{eff} slightly below one, the consumption Markstein length changes sign for sufficiently rich mixtures. Consequently, for $\phi = 2$ the FDS decreases while the FCS increases with increasing stretch. A common feature observed in both figures, is that the dependence of the FDS or FCS on stretch is unique; namely, a single value of the flame speed results for any given \mathbb{K} . As further discussed below, this is due to the alignment of the normal vector at different temperature iso-surfaces within the flame zone that holds only for spherically-symmetric flames.

Figure 5 shows the difference between the FCS and FDS as a function of the stretch rate; the filled symbols correspond to the numerical results with the various stoichiometries differentiated by symbols of different color. Theoretically, the difference between the FCS and FDS given by Eq. (35) is a linear function of stretch with a positive slope that is practically independent of the mixture composition (except for the minor variations in σ). Indeed, the numerical data for all mixtures fall along straight lines of nearly equal slope, between the ones predicted for $\tilde{\lambda} = 1$ and $\tilde{\lambda} = \tilde{T}$. To trace these limiting curves, the thermal expansion parameter was set equal to $\sigma = 7.76$, which is a representative value for mixtures with $\phi = 0.8–2$ (see Table 1).

Figure 6 shows the dependence of the FCS on stretch for mixtures with $\phi = 0.8$ and $\phi = 2$, extracted from numerical

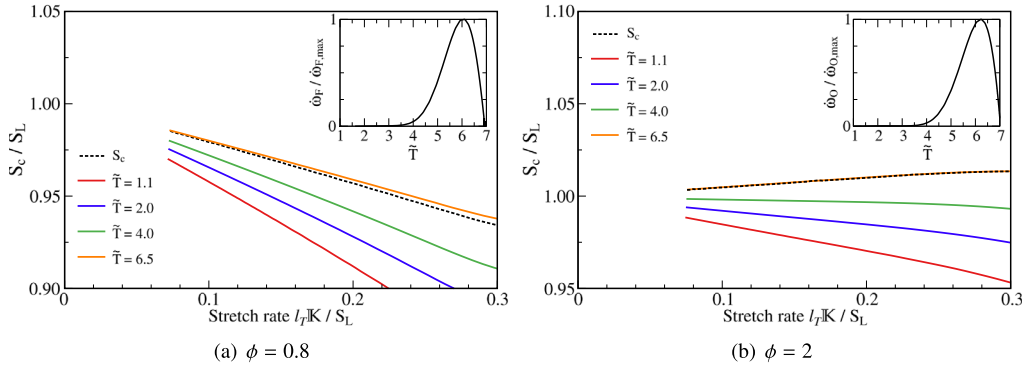


Fig. 6. The FCS determined from the global volumetric consumption rate Ω normalized by the flame surface area $4\pi R^2$ evaluated at different isotherms (solid lines), compared to the local FCS determined directly from the definition (5) (dashed lines) for lean and rich mixtures using single-step chemistry.

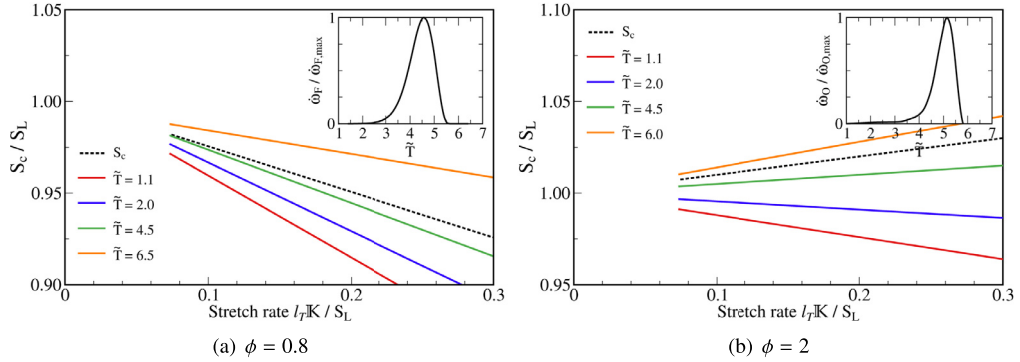


Fig. 7. The FCS determined from the global volumetric consumption rate Ω normalized by the flame surface area $4\pi R^2$ evaluated at different isotherms (solid lines), compared to the local FCS determined directly from the definition (5) (dashed lines) for lean and rich mixtures using the detailed mechanism of Qin et al. [27].

simulations using single-step chemistry in two ways. The first uses the local FCS definition (5), as already illustrated in the preceding figures, and yields a linear dependence on stretch (dashed line) consistent with the theoretical prediction (7). The second approach uses the definition (10) adopted in [18], whereby the FCS is evaluated from the global consumption rate Ω divided by the instantaneous flame surface area $4\pi R^2$. The results show that the FCS defined in this way also exhibits a linear dependence on stretch (solid curves) but with a slope that depends appreciably on the isotherm selected to calculate $R(t)$. Moreover, a poorly selected isotherm may yield a linear dependence but with an incorrect slope, as seen in Fig. 6(b). Thus, although the global consumption rate Ω is a quantity that does not suffer from any ambiguity, its normalization by the flame surface area introduces uncertainties in the numerical evaluation of the FCS and in the conclusions drawn about its dependence on flame stretch [19,20]. Our results show that when using this definition the flame surface area must be selected around the location where the fuel consumption rate $\dot{\omega}_F$ for lean mixtures, or the oxidizer consumption rate $\dot{\omega}_O$ for rich mixtures reaches its maximum value. Only at such location, corresponding to $\tilde{T} \approx 6.2$ for $\phi = 0.8$ and $\tilde{T} \approx 6.35$ for $\phi = 2$ as illustrated in the figure insets, the FCS based on Eq. (10) agrees with the results obtained using the definition (5). We note that this location, which is near the burned side of the flame, is also consistent with the asymptotic theory whereby the reaction is assumed to be confined to a sheet located where the temperature is near its maximum value.

A fundamental assumption behind the asymptotic theory is that although the true internal flame structure is determined by the detailed chemical kinetics, the global effect of aerodynamic flame stretch on flame propagation is expected to be similar for single-step and detailed chemistry descriptions and can be determined by a single lumped parameter - the Markstein length. To confirm

this hypothesis, additional calculations were performed using the detailed chemistry scheme proposed by Qin et al. [27] for lean and rich propane flames (consisting of 69 species in 463 reactions) at the limiting values of the equivalence ratio, $\phi = 0.8$ and $\phi = 2.0$. The results illustrated in Fig. 7 show that the evaluation of the FCS using the global consumption rate normalized by the flame surface area yields similar result to the direct definition (5) only when the flame surface area is evaluated at the location where the fuel/oxidizer consumption rate reaches its maximum value. The results are also in good agreement with those presented in Fig. 6 using a single-step mechanism. This demonstrates that the qualitative, and to some extent the quantitative dependence of the FCS on stretch using either a single-step or a detailed chemistry mechanism remains the same as predicted by the asymptotic theory. A similar conclusion was reached in our recent study [10] on the FDS.

In contrast to spherically expanding flames, the stationary spherical flame stabilized in the vicinity of a (spherical) porous plug burner from which the combustible mixture is ejected, is curved but not stretched. When the flame stands sufficiently far from the burner and heat losses to the porous sphere are negligible, the flame standoff distance is determined solely by the overall mass flow rate. Under such conditions, the hydrodynamic theory is valid and the flame speed, however determined, is the laminar flame speed S_L . The flame standoff distance $r = R$ is the location where the (radial) gas velocity is equal to S_L . Figure 8 shows numerical simulation results obtained by integrating the time-dependent equations to sufficiently long time, ensuring that steady state conditions have been reached. The figure displays the dependence of the FDS and FCS on the flame front curvature $\kappa = 2/R$, where it was verified that the temperature gradient at the inflow boundary for the three represented values of R is indeed negligible. The FCS, as defined in (5), is equal to the laminar flame speed for all values of κ , as it should. The FDS, on the other hand,

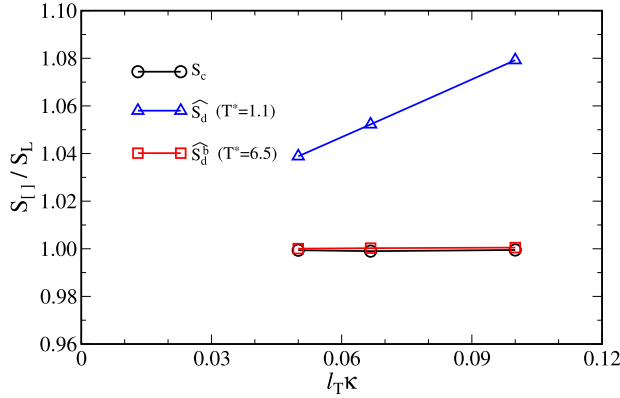


Fig. 8. The dependence of the FDS, evaluated on isotherms close to the burned (red squares) and unburned (blue triangles) side, and FCS of a stationary spherical flame (stabilized in the vicinity of a porous-plug burner) on flame front curvature, under steady conditions, based on numerical simulations for $\phi = 0.8$ using single-step chemistry. (For interpretation of the references to color in this figure legend, the reader is referred to the web version of this article.)

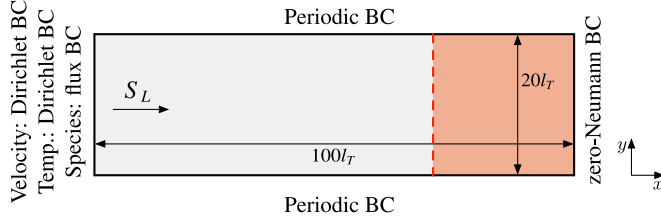


Fig. 9. The computational domain and the associated boundary conditions (BC) used in the numerical simulation of the DL-induced cusp-like flame; the shaded area marks the burned-gas region.

depends on the location used to represent the flame front. When selected near the burned side of the flame zone, the FDS remains constant and equal to S_L for all values of κ , but is erroneously predicted when evaluated at other locations within the flame zone.

6. DL-induced cusp-like flames

The rectangular domain, shown schematically in Fig. 9 for the simulation of a cusp-like flame resulting from the DL instability, is of length $100l_T$ and transverse dimension $L = 20l_T$. It is discretized using 400 and 80 spectral elements in the axial and transverse directions, respectively, and when combined with a ninth-order interpolating polynomial it results in nearly 37 points within the flame thickness l_T . In a perturbation-free environment, a planar flame will propagate in this domain along the negative x -axis at a speed S_L . It is convenient to conduct the simulations in a frame attached to the planar flame by introducing inflow at the left boundary with an axial velocity S_L . Zero-Neumann conditions are imposed at the outflow boundary and periodic boundary conditions in the transverse directions. The planar flame is perturbed initially to a small-amplitude sinusoidal profile $x = A \sin(2\pi y/L)$ with $A = 0.1$. Since the mixture composition and the selected width of the domain exceed the critical conditions for stability, the amplitude of the perturbed flame grows in time, and after a short transient evolves into a single-peak structure with a “cusp” intruding into the burned gas region. The resulting flame propagates steadily at a constant speed $U > S_L$, as predicted by Creta and Matalon [24]. The nonlinear consequence of the DL instability, was verified numerically for hydrogen-air mixtures with detailed chemistry and transport [25], and was shown to agree very well with the predictions of the hydrodynamic model. Figure 10(a) shows the temperature distribution across the perturbed planar flame corresponding

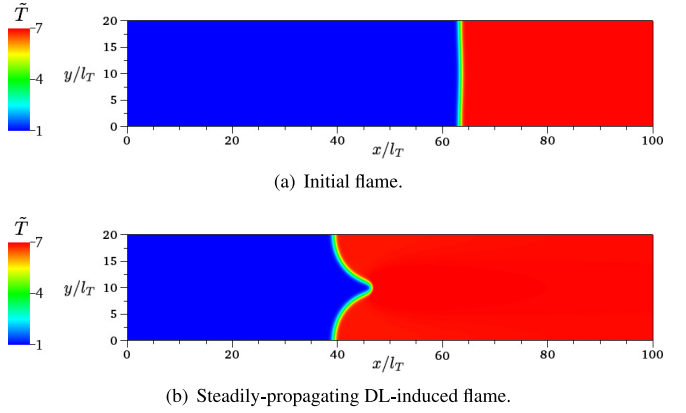
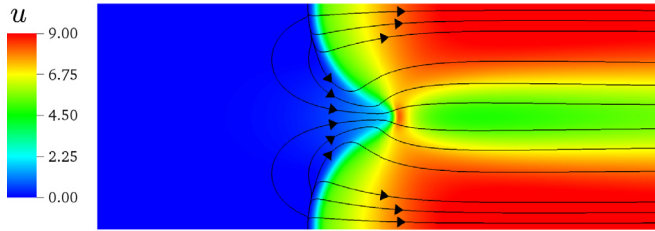


Fig. 10. Temperature distribution across (a) the initial perturbed planar flame and (b) the steadily-propagating DL-induced flame (obtained as the long-time behavior) for the propane-air mixture of equivalence ratio $\phi = 0.8$.

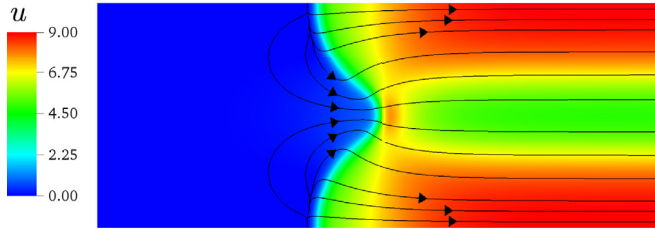
to a mixture with $\phi = 0.8$, and Fig. 10(b) shows its structure at approximately $t = 100l_T/S_L$. The figures display temperature distribution across the entire domain and clearly identify in each case the relatively thin flame separating the fresh mixture on the left from the combustion products on the right. By tracking the motion of the cusp-like structure, the flame was found to propagate at a speed $U = 1.278S_L$ (relative to the fresh mixture) which, during the simulated time, remained constant to within less than 0.1%. A similar calculation for a rich mixture with $\phi = 2$ shows the cusp-like flame propagating steadily at a speed $U = 1.298S_L$.

The same flame structure was also constructed numerically using the asymptotic hydrodynamic model, i.e., by solving the Navier-Stokes equation with the flame described as a surface propagating at a speed given by Eq. (6) using the numerical methodology described in [24,41]. The only parameters that need to be specified in this approach, in addition to the width of the domain L (hydrodynamic length scale), are the thermal expansion parameter σ and the asymptotic Markstein length \mathcal{L} ; both are available in Table 2. The Reynolds number is taken sufficiently large and equal to 10^5 to properly mimic the nearly-inviscid flow outside the flame zone. Similar to the numerical simulations, a planar flame was initially perturbed to a sinusoidal profile and the solution was monitored until steady propagation evolved. By tracking the motion of the flame the cusp-like structure was found to propagate at a speed $U = 1.181S_L$ for $\phi = 0.8$ and $U = 1.194S_L$ for $\phi = 2$. These compare well with the values extracted from the direct numerical simulations, with a difference of less than 8%. We note that the higher speed of the richer flame is due to the lower rescaled Markstein number, $\mathcal{L}/L = 0.0213$ compared to 0.0326 for the leaner flame (see Table 2), which implies a more unstable flame [24]. The flame structures obtained by these two methods (Fig. 11) agree remarkably well. The color scheme shows the variations in the axial velocity component that increases across the flame five-to-ten fold. The graphs also display streamlines that show the flow induced in the fresh mixture by gas expansion, sustaining the crest and getting deflected upon crossing the flame towards the normal to the flame surface.

Next, we examine the variations in flame stretch along the flame surface. The results below are presented for a lean mixture, but similar observations were made for all mixtures considered. In the asymptotic model, the flame front is uniquely defined and the stretch rate determined from Eq. (36) is shown in Fig. 12(a) along with its constitutive components, curvature and strain. We observe that the negative curvature and strain near the crest act together to compress the flame surface ($\mathbb{K} < 0$), while at the troughs the flame is being stretched ($\mathbb{K} > 0$) due to both positive curvature and



(a) Numerical simulations.



(b) Asymptotic hydrodynamic model.

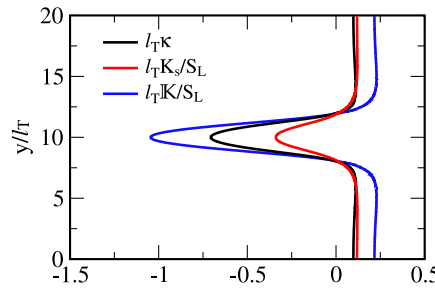
Fig. 11. Steadily propagating cusp-like flames for lean ($\phi = 0.8$) propane/air mixtures; the color scheme shows the variation in the axial velocity component and the solid lines are representative streamlines.

strain. In the numerical simulations, an iso-surface must be picked to represent the flame surface and various isotherms, ranging from $\tilde{T} = 1.01$ to $\tilde{T} = 6.5$, were thus selected. The stretch rate and its constitutive components along each isotherm are shown in Fig. 12(b) where, consistent with the discussion in Section 4, the velocity divergence was set to zero when evaluating the strain rate K_s . Although the general trend is similar to the asymptotic theory in that the flame is highly-compressed ($\mathbb{K} < 0$) near the crest and weakly-stretched ($\mathbb{K} > 0$) near the troughs, the stretch rate varies

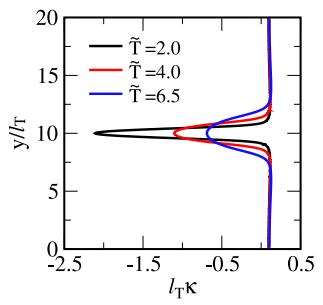
significantly across isotherms, particularly near the crest. The curvature near the crest remains always negative, but the isotherms on the burned side of the flame are smoother than the one on the unburned side, displaying a significantly lower curvature. The strain rate, on the other hand, varies from small negative to large positive values, a change that can be understood by observing the variations in the streamline pattern illustrated in Fig. 11. Near the crest the streamlines are seen first to converge, implying negative straining ($K_s < 0$) and then diverge as a result of gas expansion, corresponding to positive straining ($K_s > 0$). It should be noted that the flow ahead of the flame in the asymptotic model also displays a negative straining, while the sharp changes across the flame observed in the simulations are accounted for by satisfying the Rankine-Hugoniot jump relations.

The density-weighted displacement speed along an iso-surface $\tilde{T} = T^*$, which theoretically is given by $\hat{S}_d = S_L - \mathcal{L}_{\text{str}}^* K_s - \mathcal{L}_{\text{cur}}^* \kappa S_L$, as per Eq. (31), depends strongly on the isotherm selected to represent the flame surface. In theory, curvature and strain are uniquely defined at the flame front, a position that mimics the entire flame zone. The difference in \hat{S}_d for various isotherms within the flame zone is only due to the Markstein length, which is plotted in Fig. 13 scaled by l_f for all mixtures considered. In contrast to the curvature Markstein number $\mathcal{L}_{\text{cur}}^*/l_f$ which is well-behaved throughout the entire flame, the strain Markstein number $\mathcal{L}_{\text{str}}^*/l_f$ diverges near the unburned side and asymptotes to a constant value only near the burned side; they coincide when $\tilde{T} \rightarrow \sigma$ and are both equal to the burned Markstein number \mathcal{L}^b in this limit.

In numerical simulations (and in experiments), the variations in \hat{S}_d across the flame are also due to the large variations in strain K_s and curvature κ that we have observed. Figure 14(a) displays the theoretical displacement speed of several isotherms based on the asymptotically evaluated curvature and strain, and Fig. 14(b) illustrates the FDS extracted from the numerical simulations with curvature and strain evaluated at the specified isotherm. Relative



(a) Asymptotic hydrodynamic model.



(b) Numerical simulations.

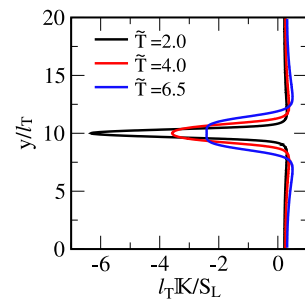
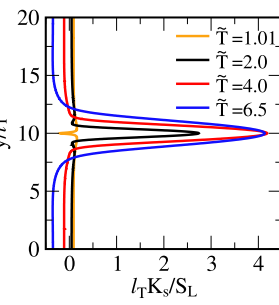


Fig. 12. Variation of the stretch rate and its constitutive components, curvature and strain, along (a) the flame front determined from the asymptotic hydrodynamic model and (b) selected isotherms obtained from numerical simulations, for a DL-induced cusp-like flame for $\phi = 0.8$. To facilitate comparison, the various quantities in the asymptotic model have been rescaled using l_f as a unit of length.

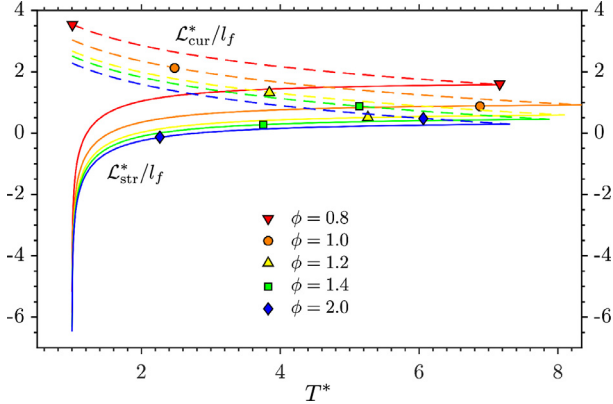


Fig. 13. Strain (solid curves) and curvature (dashed curves) Markstein numbers at various isotherms $1 < T^* < \sigma$, for selected equivalence ratios of propane/air mixtures.

to other locations within the flame zone, the FDS along isotherms sufficiently close to the unburned side of the flame is higher at the crest and lower at the troughs, which results from the exaggerated straining effects due to the large diverging value of $\mathcal{L}_{\text{str}}^*$. We conclude that the FDS evaluated at iso-surfaces on the unburned side of the flame are not reliable and should be ignored. Only when evaluated near the burned side of the flame does the FDS represents the flame behavior properly and consistently.

The burned side density-weighted FDS (corresponding to the iso-surface $\tilde{T} = 6.5$) is plotted in Fig. 15 together with the fuel and oxidizer consumption rates, for lean ($\phi = 0.8$) and rich ($\phi = 2$) mixtures. Although the FCS, as defined by Eq. (5), is an integral quantity that does not suffer from the sensitivity of selecting a specific iso-surface, the integration must be carried out across the reaction zone from the unburned to the burned state, and while the unburned state is fixed and corresponds to the composition of the fresh mixture, the burned state beyond the reaction zone is not necessarily uniform. For the results presented in Fig. 15, the fuel consumption rate was calculated from Eq. (5) with the local normal n extending a distance of $2.5l_T$ into the burned region; the oxidizer consumption rate was calculated similarly by replacing Y_F with Y_O . The comparison shows that the FDS and FCS are significantly different in magnitude and can even have different signs. Thus, unlike a planar flame where both FDS and FCS represent the propagation speed, for corrugated flames they each measure a different flame feature. Moreover, the consumption rates of fuel and oxidizer are significantly different, due to the nonuniform distribution of the excess reactant that leaks through the flame, as shown in Fig. 16. The color scheme in the figure displays variations in temperature and mass fraction of the excess reactant

for lean and rich mixtures (the scale in each graph was adjusted to make the variation near the cusp visible). For the lean mixture ($\phi = 0.8$), the flame temperature near the negatively-stretched crest is larger than its value near the positively-stretched troughs because $Le_F = 1.81 > 1$, as predicted by Eq. (28); the mass fraction of the oxidizer along the flame surface is smaller near the crest, because $Le_F - Le_0 = 0.909 > 0$, as predicted by Eq. (29). The opposite is true for the rich mixture: the flame temperature is lower at the crest, since $Le_0 = 0.901 < 1$ and the mass fraction of the fuel along the flame surface is higher at the crest because $Le_0 - Le_F = -0.909 < 0$. Thus, in order to avoid the additional ambiguity resulting from the variation in mass fraction along the flame surface, the FCS should be based on the reactant that is totally depleted in the reaction zone, namely the fuel in a lean and the oxidizer in a rich mixture.

The dependence of the flame consumption and displacement speeds on stretch is shown in Fig. 17 for lean and rich mixtures; a closeup to the region of positive stretch rates is shown in the insets. The solid lines are the theoretical predictions based on Eqs. (7) and (33), calculated with the parameters listed in Table 2. The orange/blue symbols are obtained from the simulations with the FCS based on the prescription discussed above and the density-weighted FDS refers to the isotherm $\tilde{T} = 6.5$. For the lean mixture ($\phi = 0.8$), the slope of the FDS versus stretch is negative and retains the same sign as the slope of the FCS, because \mathcal{L}^b and \mathcal{L}_c are both positive. In contrast, for the rich mixture ($\phi = 2$), the slope of \hat{S}_d versus \mathbb{K} remains positive, because $\mathcal{L}^b > 0$, but the slope of S_c vs \mathbb{K} is negative because the consumption speed Markstein length \mathcal{L}_c is now negative. The numerical results, which are based on detailed transport, reproduce this trend with good accuracy. However, unlike the asymptotic predictions that the relations between the flame speed S_f^b and stretch, and the flame consumption speed S_c and stretch, are linear, the numerical results show a nonlinear multi-valued relation for some stretch rates. The points marked by grey symbols deviate from the expected linear dependence and are characterized by two distinct values of FDS and FCS for the same stretch rate \mathbb{K} . The anticipated linear dependence (the dashed lines) is based on the single-valued data further constrained by the condition that FDS and FCS tend to S_L when $\mathbb{K} \rightarrow 0$, as discussed next.

The observed multi-valued behavior is associated with the fact that iso-surfaces corresponding to different temperatures are not parallel to each other, i.e., the direction of the normal varies from one isotherm to another as shown schematically in Fig. 18(a). This is markedly different than the response of a spherically-expanding flame to stretch where the flow is radial and the isotherms form a family of concentric spheres. Evidently, the misalignment of the normal has a more pronounced effect on the calculation of the FCS, which involves an integration across the reaction zone, than

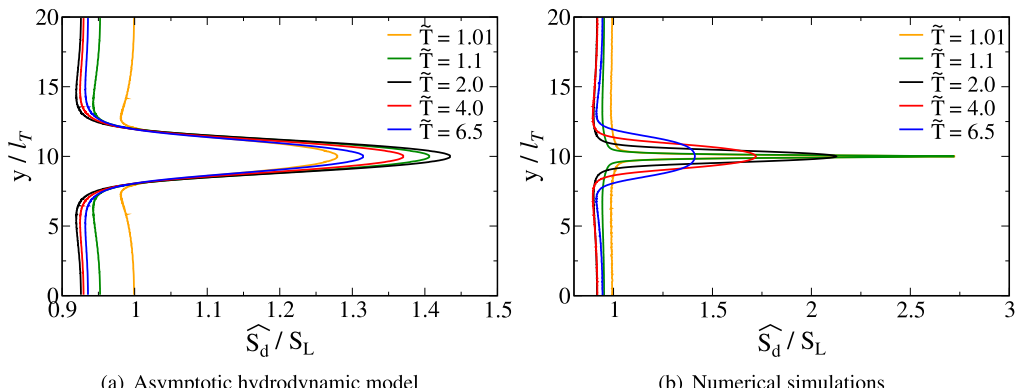


Fig. 14. Density-weighted flame displacement speed along several iso-surfaces corresponding to increasing values of temperature.

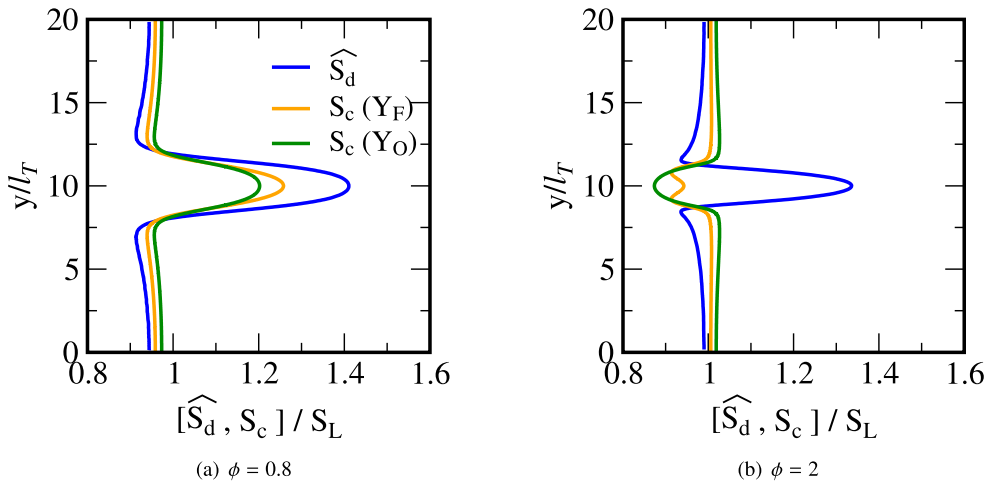


Fig. 15. Variations of fuel (orange) and oxidizer (green) consumption rates along the surface of a DL-induced cusp-like flame, for lean and rich mixtures. (For interpretation of the references to color in this figure legend, the reader is referred to the web version of this article.)

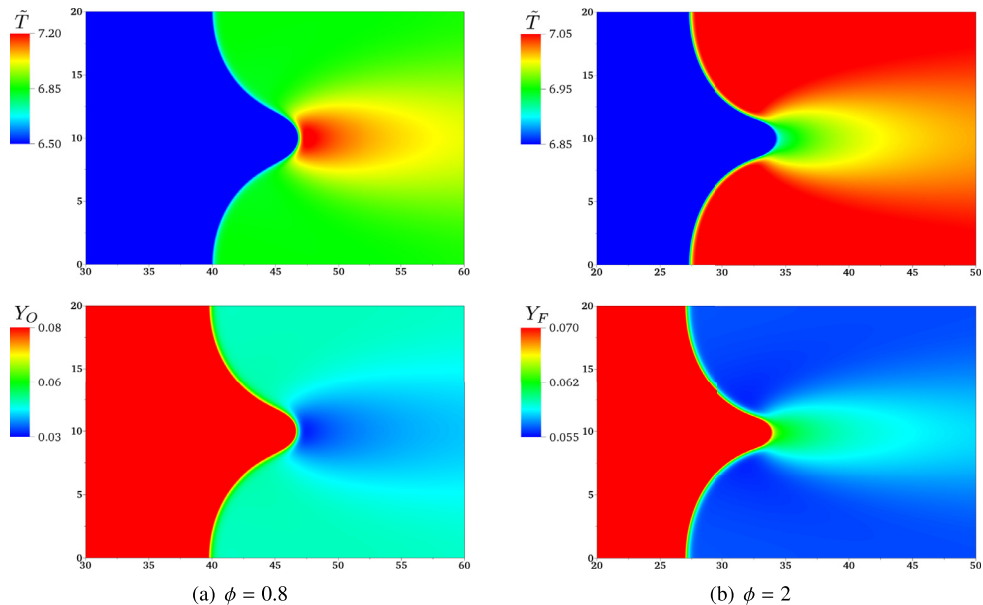


Fig. 16. Variations of temperature (top) and mass fraction (bottom) of the excess reactant across a DL-induced cusp flame, for lean and rich mixtures; the scale has been adjusted to enhance visibility.

the FDS. To clarify this issue, we devised an algorithm to quantify the extent of misalignment across isotherms throughout the flame. Starting with a point along the iso-surface $T = T_b$ representing the burned edge of the flame zone, the point along the local normal intersecting a specified isotherm $T = T^*$ is identified, as shown in Fig. 18(a). The unit normal vector \mathbf{n}^* at this point is then calculated and its slope is compared to the slope formed by the unit normal to the burned iso-surface \mathbf{n}_b . Figure 18(b) shows the slopes α_{n_b} and α_{n_u} of the vectors normal to the burned ($T_b = 6.5 T_u$) and unburned ($T^* = 1.5 T_u$) iso-surfaces, respectively, as a function of the normalized flame arc-length s . The two slopes differ significantly in the crest region where $0.3 < s/s_{\max} < 0.7$, except for the center-line point due to symmetry, and are identical elsewhere, implying that only near the troughs the isotherms remain parallel to each other.

The algorithm was implemented for lean ($\phi = 0.8$) and rich ($\phi = 2$) mixtures and the points along the flame surface were marked according to whether the misalignment between the burned and unburned isotherms exceeds a specified threshold. The results are shown in Fig. 19. The flame surface is selected as

the burned isotherm corresponding to $\tilde{T} = 6.5$. The grey-colored points correspond to $|\alpha_{n_b} - \alpha_{n_u}| > 0.03$ and those in blue to points where the difference is negligibly small. When retaining the points where the iso-surfaces are nearly parallel, i.e., the points marked in blue, the linear relations between the FCS and FDS and flame stretch are recovered, as shown by the dashed lines in Fig. 17. This approach successfully identifies flame segments where integration along a single normal direction may lead to erroneous results and excludes them from the comparison with the asymptotic results. It should be noted, however, that the approach proposed in [17] for turbulent expanding flames, which uses a varying normal vector through the flame zone, can be an appropriate way to integrate across the flame and include these additional flame segments.

Figure 20 shows the dependence of $\xi_c - \hat{\xi}_d$ on the stretch rate, for lean ($\phi = 0.8$) and rich ($\phi = 2$) mixtures. As noted earlier, the difference between the FCS and FDS given by Eq. (35) depends linearly on stretch with a positive slope that is practically independent of the mixture composition, except for the small variations in σ . Indeed, the dependence of $\xi_c - \hat{\xi}_d$ on stretch is linear with a slope ≈ 0.06 for both mixtures. The agreement with theory is

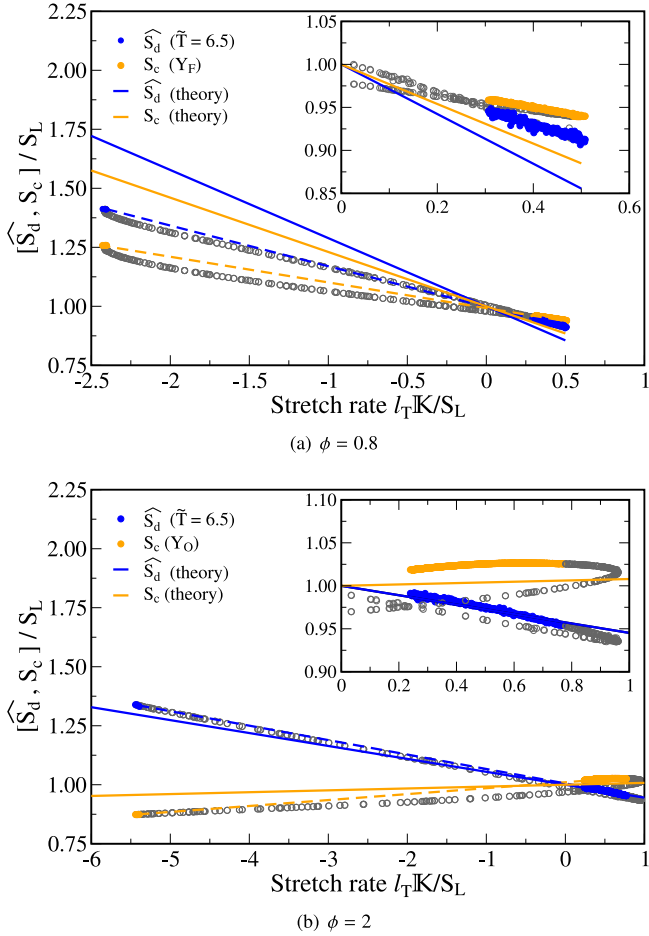


Fig. 17. The dependence of the FCS (orange) and FDS (blue) on stretch; solid lines correspond to the theoretical expressions and symbols to numerical simulations. The grey symbols denote points that should be disregarded due to the ambiguity in the determination of the FCS and replaced by the dashed line. (For interpretation of the references to color in this figure legend, the reader is referred to the web version of this article.)

much better than in Fig. 17, because it does not require estimating the Lewis and Zel'dovich numbers.

Next, we examine the relation between the overall propagation speed U , determined so far by tracking the flame in time, to the global consumption rate Ω . Integrating the fuel mass fraction equation throughout the entire combustion volume, assuming zero flux

Table 3

The propagation speed U of a steadily propagating cusp-like flame (relative to a fixed coordinate system), scaled by the laminar flame speed S_L , computed by various methods, for lean ($\phi = 0.8$) and rich ($\phi = 2$) mixtures.

	$\phi = 0.8$	$\phi = 2$
Numerical simulations		
Determined by tracking the flame in time	1.27774	1.29853
Determined by integrating the fuel consumption rate over the entire volume	1.27735	1.29843
Determined by integrating the local FCS over the flame surface	1.27790	1.29831
Hydrodynamic model		
Determined by tracking the flame in time	1.18075	1.19428
Determined by integrating the local FCS over the flame surface	1.18075	1.19428

through the lateral boundaries and a negligible flux at the outflow, one finds

$$U = \frac{1}{\rho_u (Y_{F,u} - Y_{F,b})} \frac{1}{L} \int_V \dot{\omega}_F dV = \frac{1}{A} \Omega, \quad (38)$$

so that the propagation speed U can be also determined by normalizing the global consumption rate with the cross sectional area A of the domain (here, width L). To verify this relation, Ω was obtained by (i) integrating the fuel consumption rate throughout the entire combustion volume as per Eq. (8), and (ii) integrating the local consumption speed along the flame surface A_f , as per Eq. (9) with the flame surface selected near the isotherm where the fuel consumption rate reaches its maximum, as discussed earlier (see also Fig. 6). The results for lean ($\phi = 0.8$) and rich ($\phi = 2$) flames presented in Table 3, show that all definitions yield consistent and accurate results up to the third decimal digit, and justify a posteriori the choice of the burned isotherm in determining the flame surface area. Shown in the table are also results of the asymptotic hydrodynamic model, where the comparison is made between U obtained by tracking the flame surface and obtained from Eq. (10). It is remarkable that the two are identical within the considered accuracy despite being obtained through two independent routes. Eq. (10) relies on an accurate representation of S_c , which depends on properly identifying the flame surface, complying with the asymptotic expression (7) and computing the stretch rate along the flame using Eq. (36), all of which validate the accuracy of the asymptotic expressions. Compared to the numerical simulations, the hydrodynamic model underestimates the propagation speed by 7%, but qualitatively agrees with the computational predictions very well.

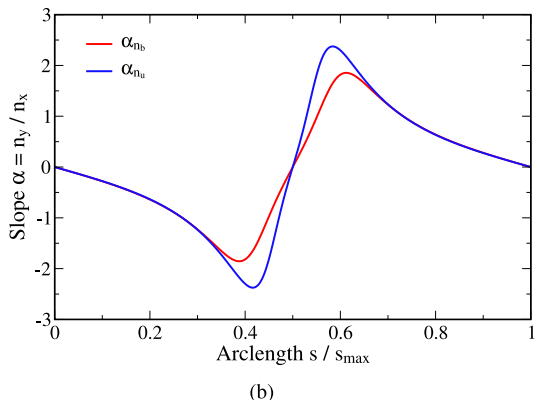


Fig. 18. (a) Schematic of the misalignment of the normal to two remote iso-surfaces, and (b) comparison of the slopes of the normal to the burned and unburned iso-surfaces as a function of the arc-length along the flame, for $\phi = 0.8$.

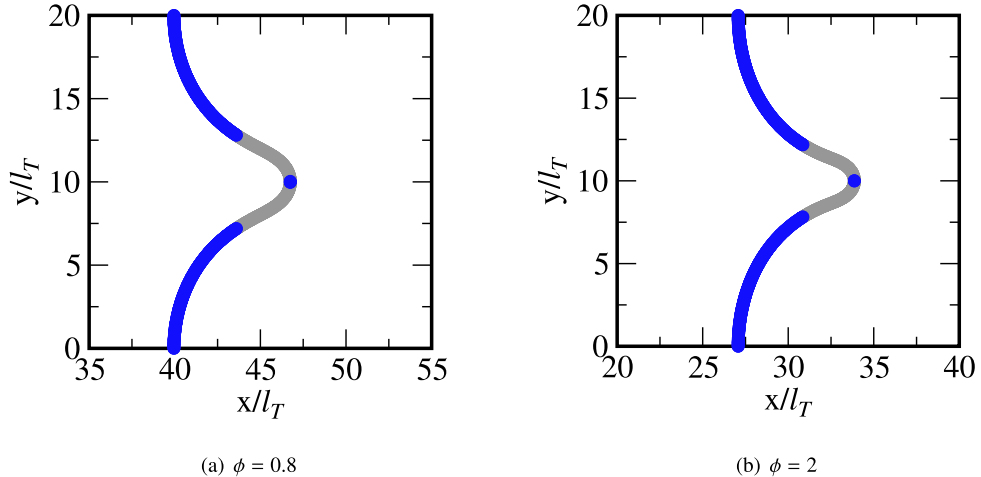


Fig. 19. Flame surface corresponding to the burned isotherm $\tilde{T} = 6.5$. The points along the surface are marked according to whether the misalignment between the burned and unburned isotherms exceeds a specified threshold; grey points correspond to $|\alpha_{n_b} - \alpha_{n_u}| > 0.03$ and blue points to $|\alpha_{n_b} - \alpha_{n_u}| < 0.03$. (For interpretation of the references to color in this figure legend, the reader is referred to the web version of this article.)

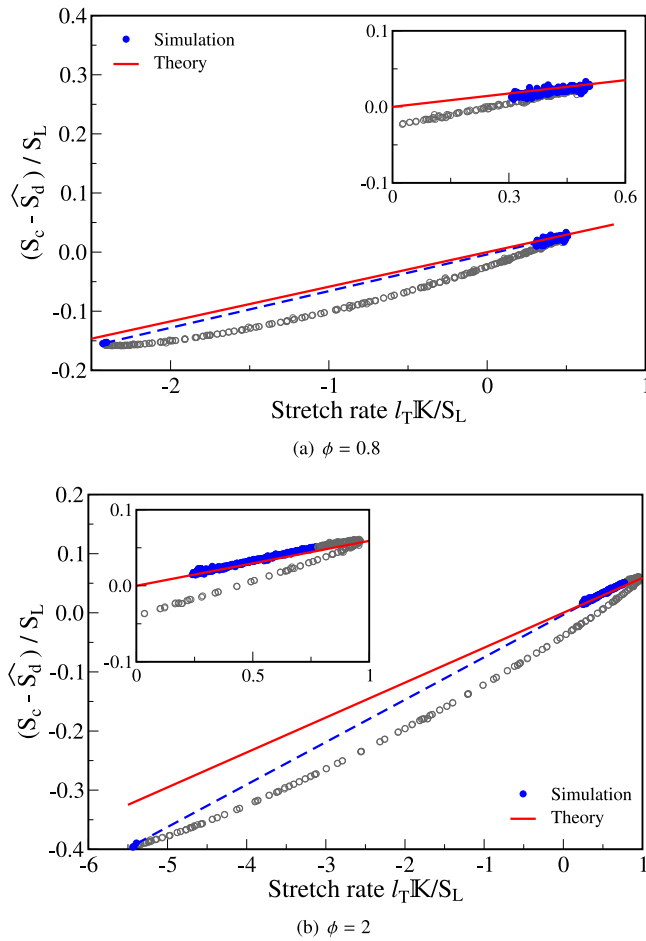


Fig. 20. The dependence of $S_c - \hat{S}_d$ on stretch; solid lines correspond to the theoretical expressions, and symbols/dashed lines to numerical simulations. The grey symbols denote points that should be disregarded due to the ambiguity in the determination of the FCS and replaced by the dashed line.

7. Conclusions

The flame displacement (FDS) and flame consumption speed (FCS) are commonly used in numerical studies that resolve the

flame region to characterize the dynamics despite the ambiguities in their definition; the FDS is associated with the displacement of an arbitrarily selected iso-surface and the FCS is an integrated quantity across isotherms that are not always parallel throughout a region that needs to be specified. The uncertainty is most significant in corrugated and turbulent flames because of the frequent highly curved regions and the flow non-uniformities created by gas expansion. In this study, a detailed comparison between numerical simulations and predictions of the asymptotic theory of weakly stretched flames was carried out in order to identify the way to utilize these properties consistently and meaningfully. An additional outcome of this comparison is the validation of the asymptotic expressions that display the dependence of the FDS and FCS on stretch, which have often been overlooked in the literature and replaced by ad-hoc expressions. The comparison shows an excellent agreement when the numerical simulations are carried out in a consistent manner with the theory. Two configurations were examined: a spherically-expanding flame where the flow is unidirectional but unsteady, and a steadily-propagating two-dimensional cusp-like flame which is spatially varying and the flow through the flame is highly nonuniform. The following conclusions are drawn from our investigation:

- The FDS and FCS are two distinct properties that describe different flame characteristics. They are equal only for planar flames in which case they determine the burning velocity.
- In the asymptotic theory the flame speed (equivalent to the FDS) and the flame consumption speed are uniquely defined by Eqs. (4) and (5), and given by $S_f = S_L - L\mathbb{K}$ and $S_c = S_L - L_c\mathbb{K}$. Both exhibit a linear dependence on stretch, but with different proportionality coefficients, or Markstein lengths.
- The asymptotic Markstein length L defined by (30) does not correspond to any specific iso-surface within the flame zone and should be used only when the flame is treated as a hydrodynamic discontinuity.
- Calculation of the local FCS from its definition (7) is straightforward when the orientation of the normal to the flame surface, properly selected on the burned side of the flame, is nearly uniform. Spherically-expanding flames are atypical because the flow is unidirectional and the normal to the various isotherms are aligned along the radial direction. The misalignment of the normal to consecutive isotherms across highly-corrugated flames leads to a multi-valued response that should not be taken into account.

- Calculation of the FDS is highly dependent on the iso-surface selected to represent the flame surface. Expressions of the density-weighted FDS for various isotherms $T = T^*$ of the form $\hat{S}_d = S_L - \mathcal{L}_{\text{str}}^* K_s - \mathcal{L}_{\text{cur}}^* S_L$ exhibit separate dependencies on strain and curvature, with distinct Markstein lengths $\mathcal{L}_{\text{str}}^*$ and $\mathcal{L}_{\text{cur}}^*$. The curvature Markstein length $\mathcal{L}_{\text{cur}}^*$ is well-behaved for all temperatures, but the strain Markstein length $\mathcal{L}_{\text{str}}^*$ becomes singular at the cold side of the flame, implying that the FDS evaluated at iso-surfaces at the unburned side of the flame are physically meaningless. The proper choice of the isotherm to represent the flame surface for the evaluation of the FDS must be near the burned side of the flame. The burned density-weighted FDS takes the form $\hat{S}_d^b = S_L - \mathcal{L}^b \mathbb{K}$, with the burned Markstein length \mathcal{L}^b given by (32).
- Calculation of the stretch rate using the expression involving curvature and strain is highly dependent on the iso-surface selected to represent the flame front, because the rate of volume dilatation vanishes only near the two ends of the flame zone. In order to obtain a unique value consistent with the theory, as given by (36), the additional constraint $\nabla \cdot \mathbf{v} = 0$ must be imposed when evaluating the strain rate K_s .
- The burned and consumption Markstein lengths may exhibit opposite behaviors with respect to stretch. Moreover, the difference between the two values, given by (34), is independent on the Lewis and Zel'dovich numbers and thus practically independent of the mixture composition. The dependence of $S_c - \hat{S}_d^b$ on stretch, which is free from the sensitivity associated with mixture properties, may therefore be used for validation.
- The global (volumetric) consumption rate Ω , obtained by integrating the rate of reactant consumption over the entire combustion volume is a well-defined property that does not suffer from any ambiguity. It has been often normalized by the flame surface area, when the flame shape is obvious as in spherical flames, to produce a quantity with dimensions of speed, which has been referred to as the FCS. This unfortunate definition introduces uncertainty in numerical simulations that stems from identifying the appropriate iso-contour to evaluate the surface area, and leads to dubious results concerning the dependence of the FCS on stretch. To obtain results commensurate with the definition (5) and consistent with the theory, the flame surface area to normalize the global consumption rate must be determined from the iso-surface corresponding to the location where the consumption rate of the deficient reactant in the mixture reaches its maximum value.

Acknowledgment

Financial support by the [Swiss Competence Center for Energy Research](#) - Efficient Technologies and Systems for Mobility (SCCER Mobility) is gratefully acknowledged (GKG).

Appendix A

Below, we follow the discussion of Poinsot and Veynante [18] on the determination of the consumption speed of a spherically expanding flame, but provide a rigorous account of the flame thickness effects from the asymptotic solution of the internal flame structure. The result agrees with the general expression (7) for FCS derived for weakly stretched flames of general shape.

Conservation of mass of the entire mixture, and the mass balance equation of the fuel (in dimensional form) are

$$\frac{\partial \rho}{\partial t} + \nabla \cdot \rho \mathbf{v} = 0$$

$$\frac{\partial}{\partial t} (\rho Y_F) + \nabla \cdot (\rho (\mathbf{v} + \mathbf{V}_F) Y_F) = \dot{\omega}_F$$

where \mathbf{V}_F is the diffusion velocity; all other symbols are defined in the main text. Subtracting the second equation from the first multiplied by $Y_{F,u}$, then integrating the result over a large fixed volume \mathbb{V} and using the divergence theorem, yields

$$\begin{aligned} \frac{\partial}{\partial t} \int_{\mathbb{V}} \rho (Y_{F,u} - Y_F) dV \\ + \int_{\mathbb{S}} [\rho (Y_{F,u} - Y_F) (\mathbf{v} \cdot \mathbf{n}) - \rho Y_F (\mathbf{V}_F \cdot \mathbf{n})] dS = - \int_{\mathbb{V}} \dot{\omega}_F dV \end{aligned} \quad (\text{A.1})$$

where \mathbb{S} is the surface of the domain. For a sufficiently large sphere, the contribution of the surface integral vanishes because $Y_F = Y_{F,u}$ and the diffusion fluxes are negligible.

Consider now a spherically-expanding flame and assume first that the flame is infinitesimally thin. Since the flame front $r = R(t)$ encloses a sphere of burned gases (with possibly residual fuel) outside of which $Y_F = Y_{F,u}$, the integral on the left hand side can be evaluated to give

$$4\pi R^2 \left(\frac{\rho_b}{\rho_u} \right) \dot{R} = - \underbrace{\frac{1}{\rho_u (Y_{F,u} - Y_{F,b})} \int_{\mathbb{V}} \dot{\omega}_F dV}_{\Omega} \quad (\text{A.2})$$

implying that the FCS defined as $S_c = \Omega / 4\pi R^2$ is, for an infinitesimally-thin flame, equal to the density-weighted burned displacement speed $\hat{S}_d^b = (\rho_b / \rho_u) \dot{R}$. Clearly, this result needs to be corrected for the processes occurring inside the flame zone. Poinsot and Veynante [18] provided an estimate for these effects by assuming average properties for all variables, later revisited by Bonhomme et al. [19] and others. A rigorous account of these changes, for weakly-stretched flames, can be obtained directly from the asymptotic solution of the internal flame structure; albeit thin, the flame has a finite thickness. The additional contribution to the volume integral on the left hand side of Eq. (A.1) from the flame zone is

$$\begin{aligned} 4\pi \frac{\partial}{\partial t} \int_{R^-}^{R^+} \rho (Y_{F,u} - Y_F) r^2 dr \\ \sim 4\pi l_f \frac{\partial}{\partial t} \left(R^2 \int_0^{-\infty} \rho (Y_{F,u} - Y_F) \tilde{\lambda}(\eta) d\eta \right) \end{aligned}$$

where η is the stretched coordinate defined in Eq. (24) with $n = R(t) - r$. This integral can now be evaluated using $\rho = \rho_u / [1 + (\sigma - 1)\Theta]$ and $Y_F = Y_{F,u}(1 - \Theta)$, with $\Theta \sim e^\eta$, giving

$$4\pi l_f \rho_u Y_{F,u} \frac{\partial}{\partial t} \left(R^2 \int_{-\infty}^0 \frac{\tilde{\lambda}(\eta) e^\eta}{1 + (\sigma - 1)e^\eta} d\eta \right) = 4\pi l_f \rho_u Y_{F,u} \frac{\gamma_1}{\sigma} 2R \dot{R}$$

where the change of variable $1 + (\sigma - 1)e^\eta = x$ was made in evaluating the integral. When added to the left hand side of (A.2), one finds

$$\Omega = 4\pi R^2 \left(\frac{\dot{R}}{\sigma} + l_f \frac{\gamma_1}{\sigma} \frac{2\dot{R}}{R} \right). \quad (\text{A.3})$$

Using the asymptotic result $\dot{R} = \sigma (S_L - \mathcal{L}^b \mathbb{K})$ for the propagation speed [10, Eq. (23)], the definition $2\dot{R}/R = \mathbb{K}$ and the relation $(\gamma_1/\sigma)l_f = \mathcal{L}_c - \mathcal{L}^b$ from (34), the global consumption rate $\Omega = 4\pi R^2 (S_L - \mathcal{L}_c \mathbb{K})$. The FCS defined from $S_c = \Omega / 4\pi R^2$ is thus given by $S_c = S_L - \mathcal{L}_c \mathbb{K}$, as derived in Section 2 for weakly-stretched flames of general shape. Hence, the dependence on stretch of the FCS and the density-weighted FDS is markedly different, with $S_c - \hat{S}_d^b = (\mathcal{L}^b - \mathcal{L}_c) \mathbb{K}$, a difference that is being masked when using ad-hoc approximations. Moreover, as discussed in Section 5, the numerical evaluation of S_c from the global consumption rate, or equivalently from Eq. (A.3), is highly sensitive to the choice of $R(t)$ used to evaluate the flame surface area. Numerical simulations using both a one-step reaction and a detailed chemistry scheme show that the proper choice consistent with the theory is the location where the consumption rate (of the deficient reactant in the mixture) reaches its maximum value.

References

- [1] B. Karlovitz, D. Denniston, D. Knapschafer, F. Wells, Studies on turbulent flames: A. Flame propagation across velocity gradients; B. Turbulence measurement in flames, *Symp. (Int.) Combust.* 4 (1953) 613–620.
- [2] A. Klimov, Laminar flames in a turbulent flow, *Zhur Priki Mekh Tekhn Fiz* 3 (1963) 49–58.
- [3] B. Lewis, G. von Elbe, *Combustion, flames and explosions in gases*, Academic Press, 1961.
- [4] J.D. Buckmaster, The quenching of two-dimensional premixed flames, *Acta Astronautica* 6 (1979) 741–769.
- [5] M. Matalon, B.J. Matkowsky, Flames as gasdynamics discontinuities, *J Fluid Mech* 124 (1982) 239–259.
- [6] P. Clavin, G. Joulin, Premixed flames in large scale and high intensity turbulent flow, *J. de Phys. Lett.* 44 (1983) 1–12.
- [7] J.K. Bechtold, M. Matalon, The dependence of the Markstein length on stoichiometry, *Combust. Flame* 127 (2001) 1906–1913.
- [8] G. Markstein, *Nonsteady flame propagation*, McMillan Publication, New York, 1964.
- [9] M. Matalon, On flame stretch, *Combust. Sci. Tech.* 31 (1983) 169–181.
- [10] G. Giannakopoulos, A. Gatzoulis, C. Frouzakis, M. Matalon, A. Tomboulides, Consistent definitions of "Flame Displacement Speed" and "Markstein Length" for premixed flame propagation, *Combust. Flame* 162 (4) (2015) 1249–1264.
- [11] C. Wu, C. Law, On the determination of laminar flame speeds from stretched flames, *Proc. Combust. Inst.* 20 (1985) 1941–1949.
- [12] D. Dowdy, D. Smith, S. Taylor, The use of expanding spherical flames to determine burning velocities and stretch effects in hydrogen/air mixtures, *Proc. Combust. Inst.* 23 (1990) 325–332.
- [13] I. Mclean, D. Smith, S. Taylor, The use of carbon monoxide/hydrogen burning velocities to examine the rate of the CO + OH reaction, *Proc. Combust. Inst.* 25 (1994) 749–757.
- [14] D. Bradley, P.H. Gaskell, X. Gu, Burning velocities, Markstein lengths, and flame quenching for spherical methane-air flames: a computational study, *Combust. Flame* 104 (1–2) (1996) 176–198.
- [15] G. Groot, L. de Goey, A computational study on propagating spherical and cylindrical premixed flames, *Proc. Combust. Inst.* 29 (2002) 1445–1451.
- [16] F. Thiesset, F. Halter, C. Bariki, C. Lapeyre, C. Chauveau, I. Gokalp, et al., Isolating strain and curvature effects in premixed flame/vortex interactions, *J. Fluid. Mech.* 831 (2017) 618–654.
- [17] J. van Oijen, G. Groot, R. Bastiaans, L. de Goey, A flamelet analysis of the burning velocity of premixed turbulent expanding flames, *Proc. Combust. Inst.* 30 (2005) 657–664.
- [18] T. Poinsot, D. Veynante, *Theoretical and numerical combustion*, 2nd, R.T. Edwards, Inc., 2005.
- [19] A. Bonhomme, L. Selle, T. Poinsot, Curvature and confinement effects for flame speed measurements in laminar spherical and cylindrical flames, *Combust. Flame* 160 (2013) 1208–1214.
- [20] A. Lefebvre, H. Larabi, V. Moureau, E. Varea, V. Modica, B. Renou, Formalism for spatially averaged consumption speed considering spherically expanding flame configuration, *Combust. Flame* 173 (2016) 235–244.
- [21] M. Matalon, C. Cui, J. Bechtold, Hydrodynamic theory of premixed flames: effects of stoichiometry, variable transport coefficients and arbitrary reaction orders, *J. Fluid Mech.* 487 (2003) 179–210.
- [22] P. Clavin, P. Garcia, The influence of the temperature dependence of diffusivities on the dynamics of flame fronts, *Journal de Mécanique Théorique et Appliquée* 2 (2) (1983) 245–263.
- [23] Y. Rastigjev, M. Matalon, Nonlinear evolution of hydrodynamically unstable premixed flames, *J. Fluid Mech.* 554 (2006a) 371–392.
- [24] F. Creta, M. Matalon, Strain rate effects on the nonlinear development of hydrodynamically unstable flames, *Proc. Combust. Inst.* 33 (2011) 1087–1094.
- [25] C.E. Frouzakis, N. Fogla, A.G. Tomboulides, C. Altantzis, M. Matalon, Numerical study of unstable hydrogen/air flames: shape and propagation speed, *Proc. Combust. Inst.* 35 (2015) 1087–1095.
- [26] J. Kim, K. Kim, S. Won, O. Fujita, J. Takahashi, S. Chung, Numerical simulation and flight experiment on oscillating lifted flames in coflow jets with gravity level variation, *Combust. Flame* 145 (2006) 181–193.
- [27] Z. Qin, V. Lissianski, H. Yang, W. Gardiner, S. Davis, H. Wang, Combustion chemistry of propane: a case study of detailed reaction mechanism optimization, *Proc. Combust. Inst.* 28 (2000) 1663–1669.
- [28] R. Kee, J. Grcar, M.S. Miller, J. Miller, PREMIX: a fortran program for modeling steady laminar one-dimensional premixed flames, *Tech. Rep.*, SAND85-8240, 1985.
- [29] A. Patera, A spectral element method for fluid dynamics: laminar flow in a channel expansion, *J. Comp. Phys.* 58 (1984) 468–488.
- [30] M. Deville, P. Fischer, E. Mund, *High-order methods for incompressible fluid flows*, Cambridge University Press, 2002.
- [31] Fischer P., Lottes J., Kerkemeier S., nek5000 web page. 2008. URL <http://nek5000.mcs.anl.gov>.
- [32] A. Tomboulides, J. Lee, S. Orszag, Numerical simulation of low Mach number reactive flows, *J. Sci. Comput.* 12 (1997) 139–167.
- [33] G.D. Byrne, A.C. Hindmarsh, PVODE, an ODE solver for parallel computers, *Int. J. High Perform. Comput. Appl.* 13 (1999) 345–365.
- [34] A. Tomboulides, S. Orszag, A quasi-two-dimensional benchmark problem for low Mach number compressible codes, *J. Comp. Phys.* 146 (1998) 691–706.
- [35] R.J. Kee, F.M. Rupley, J.A. Miller, Chemkin II: a fortran chemical kinetics package for the analysis of gas-phase chemical kinetics, Report No. SAND89-8009B, Tech. Rep., Sandia National Laboratories, 1996.
- [36] R. Kee, G. Dixon-Lewis, J. Warnatz, M. Coltrin, J. Miller, A fortran computer code package for the evaluation of gas-phase multicomponent transport properties, Report No. SAND86-8246, Tech. Rep., Sandia National Laboratories, 1996.
- [37] F. Williams, A review of some considerations of turbulent flame structure, in: M. Barrere (Ed.), *Analytical and numerical methods for investigation of flow fields with chemical reactions, especially related to combustion*, AGARD Conf. Proc. No. 164 (1975), pp. 1–125.
- [38] A. Patyal, M. Matalon, Nonlinear development of hydrodynamically-unstable flames in three-dimensional laminar flows, *Combust. Flame* 195 (2018) 128–139.
- [39] J.K. Bechtold, M. Matalon, Hydrodynamic and diffusion effects on the stability of spherically expanding flames, *Combust. Flame* 67 (1987) 77–90.
- [40] G. Jomaas, C. Law, J. Bechtold, On transition to cellularity in expanding spherical flames, *J. Fluid Mech.* 583 (2007) 1–26.
- [41] Y. Rastigjev, M. Matalon, Numerical simulation of flames as gasdynamic discontinuities, *Combust. Theory Model.* 10 (3) (2006b) 459–481.